NAVAL POSTGRADUATE SCHOOL
Monterey, California

THESIS

DAMPING AND MICROSTRUCTURES

IN AGED CU-MN BASED ALLOYS

by

Joseph Patrick Heil

June 1988

Thesis Advisor: Jeff Perkins

Approved for public release; distribution is unlimited

REPORT DOCUMENTATION PAGE

1a. REPORT SECURITY CLASSIFICATION UNCLASSIFIED	1b. RESTRICTIVE MARKINGS
2. SECURITY CLASSIFICATION AUTHORITY	3. DISTRIBUTION / AVAILABILITY OF REPORT Approved for public release; distribution is unlimited
2b. DECLASSIFICATION / DOWNGRADING SCHEDULE	
4. PERFORMING ORGANIZATION REPORT NUMBER(S)	5. MONITORING ORGANIZATION REPORT NUMBER(S)
6a. NAME OF PERFORMING ORGANIZATION Naval Postgraduate School 6b. OFFICE SYMBOL (*If applicable*) Code 69Ps	7a. NAME OF MONITORING ORGANIZATION Naval Postgraduate School
6c. ADDRESS (*City, State, and ZIP Code*) Monterey, California 93943-5000	7b. ADDRESS (*City, State, and ZIP Code*) Monterey, California 93943-5000
8a. NAME OF FUNDING / SPONSORING ORGANIZATION 8b. OFFICE SYMBOL (*If applicable*)	9. PROCUREMENT INSTRUMENT IDENTIFICATION NUMBER
8c. ADDRESS (*City, State, and ZIP Code*)	10. SOURCE OF FUNDING NUMBERS PROGRAM ELEMENT NO. / PROJECT NO. / TASK NO / WORK UNIT ACCESSION NO.

11. TITLE (*Include Security Classification*)
DAMPING AND MICROSTRUCTURES IN AGED CU-MN BASED ALLOYS

12. PERSONAL AUTHOR(S)
Heil, Joseph P.

13a. TYPE OF REPORT	13b. TIME COVERED	14. DATE OF REPORT (*Year, Month, Day*)	15. PAGE COUNT
Master's Thesis	FROM _____ TO _____	1988, June	67

16. SUPPLEMENTARY NOTATION "The views expressed in this thesis are those of the author and do not reflect the official policy or position of the Department of Defense or the U.S. Government."

17. COSATI CODES		
FIELD	GROUP	SUB-GROUP

18. SUBJECT TERMS (*Continue on reverse if necessary and identify by block number*)
High Damping, Cu-Mn, Cu-Mn-Al, Specific Damping Capacity, Log Decrement, Tweed Microstructure, Flickering

19. ABSTRACT (*Continue on reverse if necessary and identify by block number*)

An aged high damping alloy 53Cu-45Mn-2Al was studied both microstructurally by transmission electron microscopy (TEM) and macrostructurally with two different damping measurement methods. In-situ heating and cooling observations were made with TEM in order to define the recently discovered "flickering" phenomenon associated with it's "tweed" microstructure. TEM studies were also made of an aged 53.6Cu-46.4Mn binary alloy. Damping measurements were obtained by a normalized bandwidth method applied to data from a resonant bar. This was used to determine (i) the aging condition for optimum damping, (ii) the subsequent trend of damping at room temperature for each aging condition, and (iii) the effect of an 8 HR storage at 100°C on damping capacity. Damping measurements utilizing a free decay technique to determine log decrement were also used and compared to results from the normalized bandwidth method.

20. DISTRIBUTION / AVAILABILITY OF ABSTRACT	21. ABSTRACT SECURITY CLASSIFICATION
☒ UNCLASSIFIED/UNLIMITED ☐ SAME AS RPT. ☐ DTIC USERS	Unclassified
22a. NAME OF RESPONSIBLE INDIVIDUAL Prof. Jeff Perkins	22b. TELEPHONE (*Include Area Code*) (408) 646-2216 22c. OFFICE SYMBOL Code 69Ps

Approved for public release: distribution is unlimited.

Damping and Microstructures in Aged Cu-Mn Based Alloys

by

Joseph Patrick Heil
Lieutenant, United States Navy
B.S., United States Naval Academy, 1980

Submitted in partial fulfillment of the requirements for the degree of

MASTER OF SCIENCE IN MECHANICAL ENGINEERING

from the

NAVAL POSTGRADUATE SCHOOL
June 1988

Author: Joseph Patrick Heil
Joseph Patrick Heil

Approved by: Jeff Perkins
A. J. Perkins, Thesis Advisor

A. J. Healey, Chairman
Department of Mechanical Engineering

Gordon E. Schacher
Dean of Science and Engineering

ABSTRACT

An aged high damping alloy 53Cu-45Mn-2Al was studied both microstructurally by transmission electron microscopy (TEM) and macrostructurally with two different damping measurement methods. In-situ heating and cooling observations were made with TEM in order to define the recently discovered "flickering" phenomenon associated with its "tweed" microstructure. TEM studies were also made of an aged 53.6Cu-46.4Mn binary alloy. Damping measurements were obtained by a normalized bandwidth method applied to data from a resonant bar. This was used to determine (i) the aging condition for optimum damping, (ii) the subsequent trend of damping at room temperature for each aging condition, and (iii) the effect of an 8 HR storage at 100°C on damping capacity. Damping measurements utilizing a free decay technique to determine log decrement were also used and compared to results from the normalized band width method.

TABLE OF CONTENTS

LIST OF FIGURES

ACKNOWLEDGEMENT

The author would like to acknowledge the insight, guidance, and patience of Professor Jeff Perkins, who made the course of this research enjoyable and productive. Thanks must also go to Professor Tadayoshi Yamashita for his hard work, training, and assistance. Finally, the author gives special thanks to his wife Suzanne, who provided immeasurable support, patience, and understanding during the long hours of experimentation and writing.

I. INTRODUCTION

A. INTEREST AND APPLICATIONS

The control of extraneous vibrations which are inherent in dynamic systems, and the associated reduction in noise level, is important to those who operate these systems. In the U.S. Navy, unwanted noise and vibration can reduce operator and system performance, shorten system life, and greatly increase underwater detection ranges of ships and submarines. In other words, noise reduction through vibration control can at a minimum improve operator and system overall efficiencies, and may even give a needed tactical advantage when stealth and quiet are paramount.

The two most common techniques for vibration control are system isolation and dissipation through absorption pads [Ref. 1]. However, these techniques tend to add weight, take up needed space, and are limited by physical constraints. A third method for vibration control is to replace or modify system components which would normally be fabricated from low damping materials with components that include a high damping material of otherwise similar properties. This thesis is a part of an ongoing research effort at the Naval Postgraduate School to more completely define the capabilities of commercially available high damping alloys and to understand the microstructural mechanisms involved.

B. BACKROUND

Any mechanical system which contains mass and elasticity will vibrate when subjected to force or excitation. These vibrations will decay differently with time depending on many factors, including the nature and magnitude of the excitation, temperature, system geometry, and system microstructure. Such vibrational decay is known as damping, for

which there are several common measures; such as specific damping capacity (SDC); these will be described in the next section.

As previously mentioned, the Navy has many possible applications for high damping materials and the benefits of their use could be extensive. Most commonly used materials, however, display low SDC (i.e., less than 1%) while many commercially available materials exist which have high SDC (see Table 1). A high damping material is generally defined as having an SDC greater than 20%. A high damping alloy which has been studied with great interest at the Naval Postgraduate School is an alloy based on the Cu-Mn system, with composition 53Cu-45Mn-2Al.

C. MACROSTRUCTURAL DAMPING

1. Theory

A system which has complex damping and undergoes forced vibrations can be modelled quite accurately as a mass connected to a dashpot and spring in parallel (Ref. 2, pp. 48-49). Solving the differential equation corresponding to this model yields the steady state solution for time dependent displacement y(t):

$$y(t) = Y*\exp[i(\omega t-\Phi)]$$

$$= F*\exp[i\omega t]/[(k-m\omega^2)+i\omega c] \qquad (1.1)$$

where

Y = displacement maximum amplitude
F = time dependent forcing function
Φ = phase angle between response and forcing function
ω = excitation frequency
c = viscous damping coefficient
k = spring constant
m = mass

TABLE 1

DAMPING CHARACTERISTICS OF SELECTED METALS AT ROOM TEMPERATURE [Ref. 1]

Metal	SDC (%)	Yield Strength (10^3 psi)	Density (gm/cm^3)
Magnesium (wrought)	49	26	1.74
Cu-Mn alloys (Incramute, Sonoston)	40	45	7.5
Ni-Ti alloy (Nitinol)	40	25	6.45
Fe-Cr-Al alloy (Silentalloy)	40	40	7.4
High-C gray iron	19	25	7.7
Nickel (pure)	18	9	8.9
Iron (pure)	16	10	7.86
Martensitic stainless steel	8	85	7.7
Gray cast iron	6	25	7.8
SAP (aluminum powder)	5	20	2.55
Low-carbon steel	4	50	7.86
Ferritic stainless steel	3	45	7.75
Malleable, modular cast irons	2	50	7.8
Medium-carbon steels	1	60	7.86
Austenitic stainless steel	1	35	7.8
1100 Aluminum	0.3	5	2.71
Aluminum alloy 2024-T4	<0.2	47	2.77
Nickel-based superalloys	<0.2	Range	8.5
Titanium alloys	<0.2	Range	4.5
Brasses, bronzes	<0.2	Range	8.5

For a single degree of freedom system, a good approximation of a cantilever beam, there occurs many resonant frequencies ω_n. Examples of the first three resonant frequencies, also known as modes, are shown below in Figure 1.1.

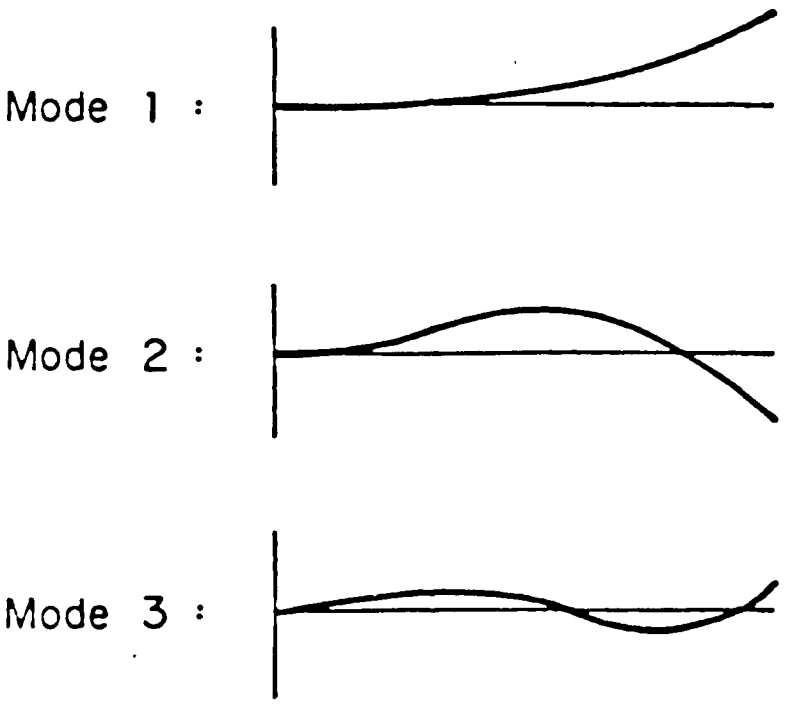

Figure 1.1 First Three Resonant Modes of a Cantilever Beam

There are a number of parameters used to characterize system damping, many of which are related. Among these are:

a. Logarithmic decrement (δ) --for exponential, cyclic, free decay [Ref. 2:pp. 30-31] (see Figure 1.2)

$$\delta = \ln(a_i/a_{i+1}) = (1/n)\ln(a_0/a_n) \qquad (1.2)$$

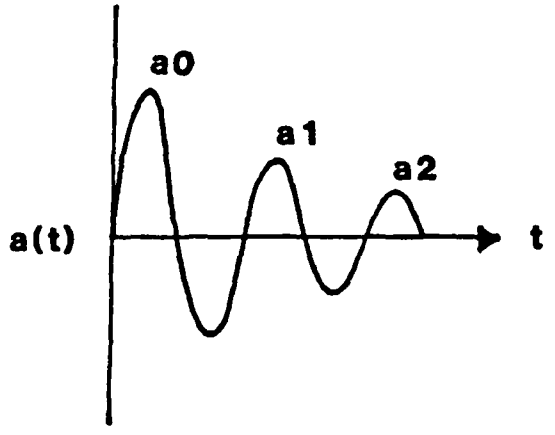

Figure 1.2 Logarithmic Decrement

b. Specific damping capacity (SDC) --for exponential, cyclic, free decay [Ref. 3:pp. 444-445] (see Figure 1.2)

$$SDC(\%) = \frac{(a_i^2 - a_{i+1}^2)*100}{(a_i^2)} \qquad (1.3)$$

c. Quality factor (Q) --for forced vibration, the resonant frequency (ω_n) divided by the difference between the two frequencies, ω_1 and ω_2, for which the stored energy is exactly half the maximum value (which occurs at ω_n- see Figure 1.3) [Ref. 2:pp. 76-77]

$$Q = \frac{\omega_n}{\omega_2 - \omega_1} \qquad (1.4)$$

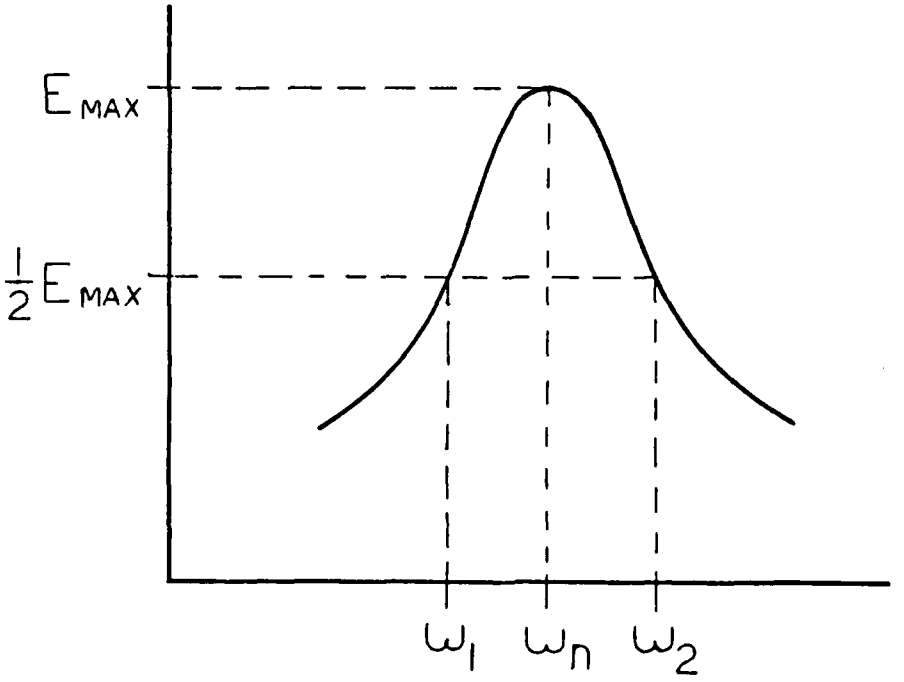

Figure 1.3 Quality Factor

d. Specific Damping Capacity (SDC)-- for forced vibration [Ref. 4: pg. 19]

$$SDC(\%) = (2\pi/Q)*100 \qquad (1.5)$$

2. Measurement Techniques

Depending on desired test parameters and sample geometry, there are many techniques available to determine the damping capacity of a material or system. At the Naval Postgraduate School the most recent and successful method is a modified version of the resonant dwell technique. In this method, a cantilever beam is subjected to continuous excitation at random frequencies surrounding the beam's first three resonant modal frequencies. Beam response is then

compared to the excitation and SDC is calculated from equation 1.5. Two of the first and most comprehensive studies utilizing this technique were by Reskusich [Ref. 4] and Dew [Ref. 5]. Measurement of both excitation and response is accomplished by accelerometers mounted at the beam root and tip respectively. A spectrum analyzer processes the response at each modal frequency, and strain information is obtained from gages mounted directly on the beam.

Dew also investigated a modification of the technique described above by utilizing a beam root strain gage for response measurement while retaining the root accelerometer for input. He found a change in response amplitude but no change in damping measurement.

Cronauer [Ref. 6] expanded test parameter capabilities by developing an apparatus which allowed damping measurements to be carried out at elevated temperature (to approximately 100°C).

The logarithmic decrement technique is a method which shows damping during free decay and can be used for a variety of strain amplitudes. A common method for low cycle decay is the use of a torsion pendulum, a recent study of which is included in a paper by Ritchie et al [Ref. 7]. Another use of log decrement is the study of oscillatory decay of a cantilever beam after being subjected to impact, investigated in this study.

D. METALLURGY OF THE CU-MN ALLOY SYSTEM

The Cu-Mn binary alloy system has been studied in great detail for more than four decades. The phase diagram was well established and has been changed very little since 1945 [Ref. 8]. A version of the Cu-Mn phase diagram with a compilation of various experimentally observed transformations in the $\alpha + \gamma$ two phase region was assembled by Mayes [Ref. 9] and is presented as Figure 1.4. It is in this two phase region that research has focused for theories on

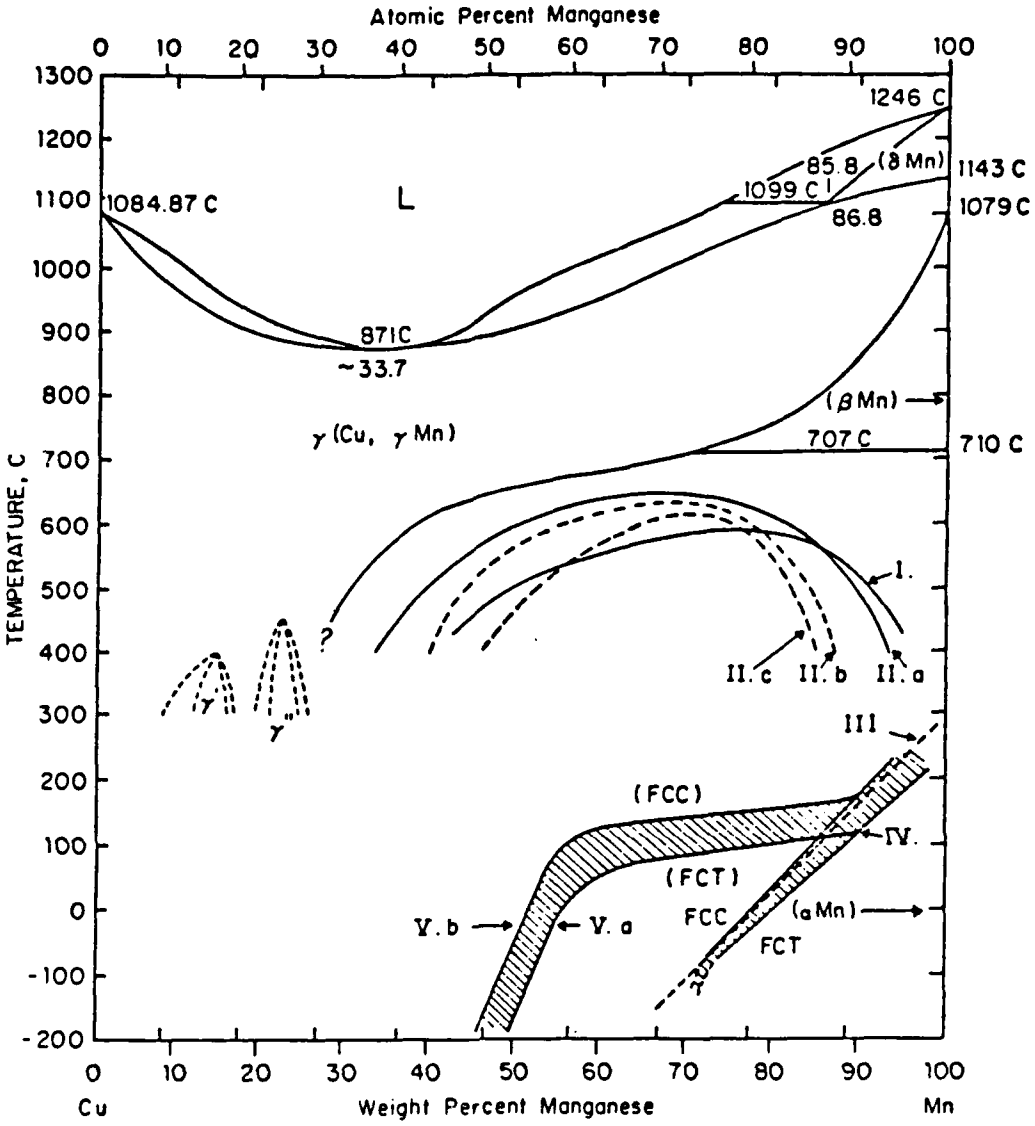

Figure 1.4 Phase Diagram of Cu-Mn Binary System with Miscibility Gap, M_S, and T_N [Ref. 9].

I. Miscibility gap [Ref. 16].

II. Miscibility gap [Ref. 17].
   a. Layering range.
   b. Chemical Spinodal.
   c. Coherent Spinodal.

III. Néel temperature [Ref. 16].

IV. FCC-to-FCT transition in quenched alloy [Ref. 18].

V. FCC-to-FCT transition in aged alloy [Ref. 19].

operative damping mechanisms. The next section will focus on these proposed mechanisms, while an overview of Cu-Mn metallurgy follows.

A broad FCC solid solution of γ-Mn exists at elevated temperature (above about 650°C for 45 wt-% Mn). Upon cooling from this FCC phase, an antiferromagnetic ordering occurs [Refs. 10-15] at a temperature which depends on the Mn content of the alloy, being higher for richer concentrations [Refs. 11, 15]. This temperature is known as the Néel temperature (T_N), and the dependence on Mn content was accurately shown by Vitek and Warlimont [Ref. 16]. With additional cooling there is a tetragonal distortion of the lattice and the alloy adopts a twinned FCT microstructure [Refs. 11,18,20,21,22]. This structure has been called quasi-martensitic and the transformation temperature, which also increases with increased Mn content, is called the martensite start (M_S) temperature [Refs. 10,11,18]. M_S is usually slightly below T_N, but for some compositions the two are essentially coincident [Refs. 18,21,22]. For alloy compositions below about 82% Mn, M_S and T_N fall below room temperature, so that samples quenched to room temperature from the γ-phase will remain FCC.

Also shown on figure 1.4 are various proposed locations of a miscibility gap, which is agreed to exist in the two phase region [Refs. 16,23,24]. When an initially homogeneous FCC sample within this range of composition is held at a temperature within the gap, there is a continuous separation of the single phase into FCC regions of differing composition, with the amplitude of the composition modulation determined by the endpoints of a tie-line across the gap at that temperature [Refs. 10,17,25,26]. In other words, there is a separation into relatively Mn-rich and Mn-poor regions, with a gradient of Mn content between them.

E. MICROSTRUCTURE OF THE CU-MN ALLOY SYSTEM

1. Damping Mechanisms

Probably the most widely held view on the source of damping in the Cu-Mn alloy system is that energy is absorbed during the movement of the twin boundries between FCT plates [Refs. 25,27,29]. Hedley [Ref. 25] also states that the reversible rotation of magnetic moments associated with each Mn ion is a contributing factor. Mayes and Perkins [Ref. 9] proposed two additional models, the first of which is directly related to the premartensitic tweed structure which is common in aged alloys, and the second concerning energy absorption by the FCC to FCT transformation as a result of stress induction under vibrational conditions.

2. Tweed Structure

"Tweed" is the generic term for a specific type of cross-hatched contrast which appears in TEM images in a variety of alloy systems. In the Cu-Mn alloy system, the lines of contrast lie approximately along traces of {110} planes of a cubic phase, obeying extinction rules which are consistent with <011> shear distortions [Refs. 30,31]. Two basic conditions are required for this type of contrast appearance to develop: (i) an elastically anisotropic matrix phase that is "soft" with respect to <011> shear distortions, and (ii) a source of finely distributed centers of asymmetric strain. Various sources of these strain centers have been identified for different systems, such as G-P zones [Ref. 30], finely distributed precipitate particles [Ref. 31], ordered domains [Ref. 32], or simply domains in which there is an incipient lattice transition that distorts the lattice [Ref. 33].

The distinction of a given tweed contrast, i.e. the sharpness of the cross hatched appearance, is quite dependent on the distribution, nature and magnitude of these strain centers, as well as the degree of anisotropy of the

matrix phase [Ref. 9]. If any of these factors is deficient, the typical cross-hatched tweed contrast appearance will not appear, and usually a somewhat "mottled" contrast will be observed. Many "tweedy" alloys, therefore, show a variation in tweed contrast with changes in distribution and/or strength of the strain centers. Such may be the case, for example, as the strain centers increase during aging [Ref. 30] or during cooling toward a temperature range of lattice instability [Ref. 34].

3. Flickering

An unusual type of TEM contrast effect was recently observed in aged 53Cu-45Mn-2Al samples that also displayed tweed contrast [Ref. 9]. This is unique in that it involves movement of certain parts of the image contrast, and has been dubbed "flickering". This effect apparently had not been observed in previous studies of either Cu-Mn or any other systems that display a tweed microstructure.

Flickering is only seen in samples sufficiently aged to also show a definite aligned tweed structure, for example, at least 4 hours at 400°C. A magnification level of at least 40,000X must be used to reveal the image movements, as the regions that flicker are on the scale of the tweed spacing, about 10 to 20 nm. In a bright field image, the flickering regions will be in the darker contrast areas and display a variety of repetitive movements such as rotation, pulsing, shifting location, splitting, or a combination of these. Repetition frequencies range from about 0.1 Hz to 10 Hz, although higher frequencies may be present but beyond visual resolution. Examples of some of the observed movements are sketched in Figure 1.5. At any one time, there are a great many flickering sites observable on the viewing screen and the variety of activity usually encompasses all the examples shown in Figure 1.5. The flickering effect has been recorded on videotape, and the most successful

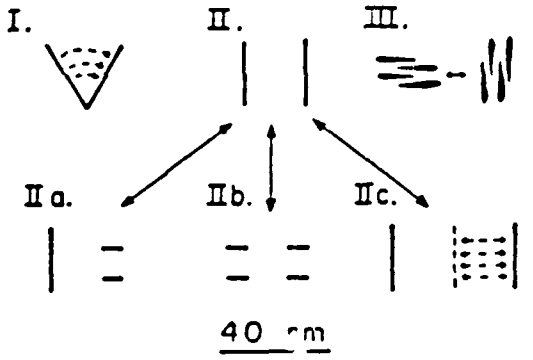

Figure 1.5 Schematic of a Variety of Observed Flickering Morphologies [Ref. 9]

photographic method to record activity has been with the weak beam technique, an example of which is shown in reference 9.

F. OBJECTIVES

In the present work, research to further characterize and understand the aged alloy 53Cu-45Mn-2Al was concentrated in two general areas, (i) macrostructural damping capabilities, and (ii) microstructural characteristics.

Previous research had shown that when aged at 400°C, the time for optimum damping appeared to be about 16 hours [Ref. 4]. Since this had been based on aging trials at times of 8, 16, and 32 hours, it was felt that a more accurate determination of optimum aging times was warranted, so that in the present research additional aging times around 16 hours were considered. Another objective was to determine the trend of damping capacity of these same variously aged alloys both at room temperature and elevated temperature. At room temperature, damping capacities and variations thereof over time periods up to 96 hours were examined. For elevated temperature, damping variations were monitored over time periods of 8 hours at 100°C, and subsequent room temperature damping was evaluated. In addition, investigation of an alternate damping capacity measurement technique, using

the log decrement parameter, was conducted for possible future use as a quick and accurate method of checking damping.

Microstructurally, TEM observations utilizing in-situ heating and cooling were made in order to gain a better understanding of both flickering and tweed contrast microstructure. A 53.6Cu-46.4-Mn binary alloy was observed under similar aging conditions to 53Cu-45Mn-2Al to better understand the possible microstructural effect of aluminum as an alloying element with copper and manganese.

II. EXPERIMENTAL PROCEDURES

A. TRANSMISSION ELECTRON MICROSCOPY

53Cu-45Mn-2Al sample material was provided by Olin Metal Research in the form of 0.25 inch thick rolled plate of nominal composition 58Cu-40Mn-2Al. Actual composition, as previously reported by Reskusich [Ref. 4], was determined by Anamet Laboratories, Berkeley, California, to be:

	Cu	Mn	Al	Zn	Si	Fe	Cr	Remain
w/o:	53.1	44.8	1.61	0.1	0.08	0.06	0.05	0.2

The plate was warm rolled into foil samples of approximately 0.35 mm thickness from which 3 mm diameter discs were punched. Discs were lightly sanded to remove surface oxide and then enclosed in sealed evacuated quartz tubes. Sealed specimens were solution treated at 800°C for two hours followed by a water quench to room temperature. Aging was done for 8 or 16 hours at 400°C, followed by a water quench and storage in a freezer maintained at -22°C until needed for observation.

Binary alloy material with a nominal composition 53.6Cu-46.4Mn was provided by S. Spooner of Oak Ridge National Laboratories in the form of a cylindrical plug, diameter 0.75 inch and length approximately 0.6 inch. It had been prepared by arc melting under vacuum 254.7 g of high grade Cu with 220.3 g of high grade Mn. Wafers of approximately 0.7 mm thickness were sliced off by low speed diamond saw, then hand sanded to 0.25 mm. Discs of 3 mm diameter were punched from the foil and sealed in evacuated quartz tubes. Solution treating and aging procedures were similar to the previous alloy, however aging times were 6, 13, 24, and 36 hours.

Thin foils for TEM observation were prepared by the methods used by Reskusich [Ref. 4] and Mayes [Ref. 9]. A detailed summary is contained in reference 9, pages 15 and 33-36. Thinning was accomplished by a two stage process utilizing both jet and static electropolishing. After removal from storage at -22°C, samples were lightly sanded to remove surface oxides. They were then placed in a lollipop holder and jet electropolished at room temperature with a solution of H_3PO_4 and H_2O, current approximately 580 ma. This creates a dimple in the center of the sample for preferential thinning during the second stage. Final thinning to perforation was performed by a static electropolish, holding the sample with platinum tipped tweezers in stirred solution of H_3PO_4 and CrO_3, voltage 8 to 12 V. TEM observation was carried out immediately after thinning on a JEOL-120CX transmission electron microscope operated at 120 kV. In-situ heating and cooling was conducted with a Gatan model 636 double tilt specimen holder loaned by Lawrence Livermore National Laboratory. This specimen holder had a temperature range of -160°C to 90°C.

B. DAMPING MEASUREMENTS

Cantilever beams previously used by Reskusich [Ref. 4] and Cronauer [Ref. 6] were reused for this research. Beam dimensions are shown in Figure 2.1.

Beams were sealed in evacuated quartz tubes and solution treated at 800°C for two hours, followed by a water quench. The beams were then aged at 400°C for 12, 14, 15, 16, 17, 18, and 20 hours. Following aging the beams were stored in a freezer at -22°C until use.

Damping measurements were conducted using a modified resonant dwell technique similar to that used by Reskusich and Cronauer, and an extremely comprehensive discussion of equipment and technique is found in reference 6, pp. 36-68.

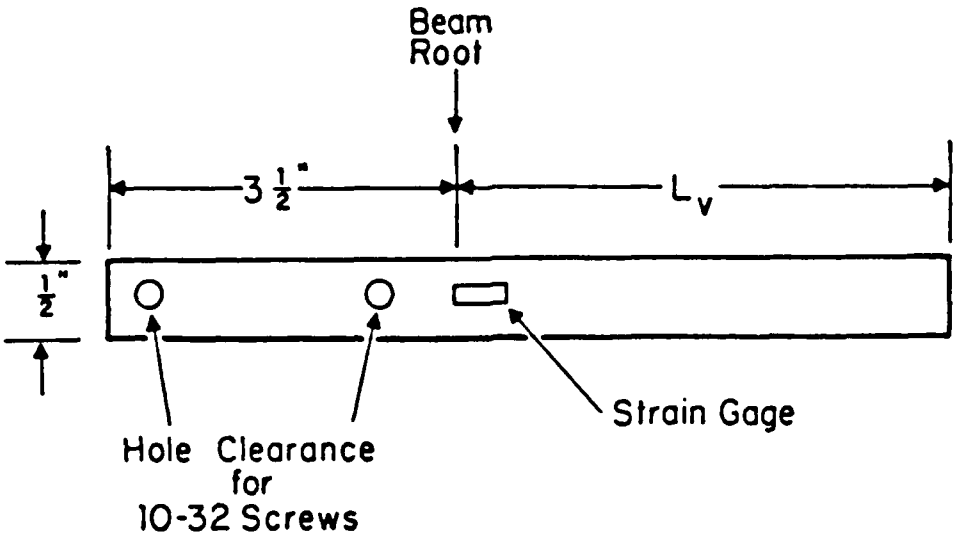

Figure 2.1 Cantilever Beam Geometry

A modification was made to this technique and will be noted during the following brief discussion.

A Scientific Atlanta SD380Z 2-channel signal analyzer was used to generate a random noise signal, which was amplified by a MB Dynamics 2125 MB power amplifier. This signal was transmitted to the clamped end of the beam by way of an air cooled MB Dynamics PM-25 Vibramate exciter connected to a "stinger" rod, which was attached directly to the base of the beam clamp. The random noise signal caused the beam to resonate and therefore undergo strain easily measurable at flexure points depending on the resonant mode. For example, strains induced by mode one resonance (and to a lesser extent higher modes) can be measured by a strain gage at the beam root, as shown by the gage depicted in Figure 2.1. It was decided to make this single strain gage the source of measured beam response as well as beam strain, while input excitation would still be measured by an accelerometer mounted on the beam clamp. Strain gages used were by Measurements Group, type CEA-13-250-UN-350; and the accelerometer used was by Endevco, model 2250A-10. This set-up

differed from Cronauer and Reskusich, who measured beam response with a second accelerometer mounted on the beam tip, and had previously been shown to be accurate by Dew [Ref. 5].

Both input and output signals were transmitted back to the signal analyzer, which (i) performs a transfer function of output over input at mode one frequencies, (ii) measures the coherence, or clarity of the received signals, and (iii) measures the strain at mode one frequencies. Specific damping capacity was calculated from the first of these by the half power point method, utilizing equations (1.4) and (1.5). Transfer function frequency response was displayed on a log scale and half power point frequencies ω_1 and ω_2 were defined by the 3 dB down points on either side of ω_n. Sample plots of both broad and narrow band transfer function and coherence are shown in Figures 2.2 and 2.3 respectively.

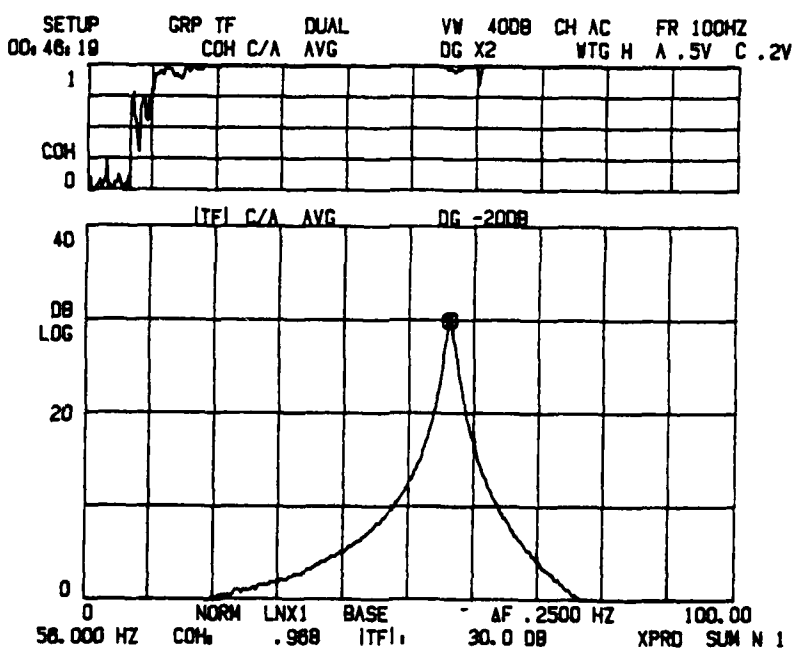

Figure 2.2 Broad Band Transfer Function and Coherence

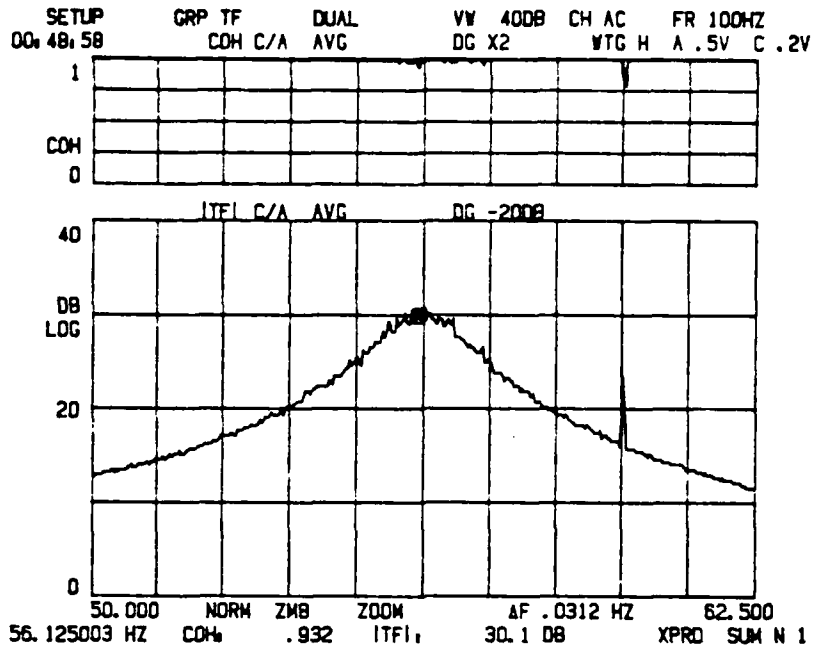

Figure 2.3 Narrow Band Transfer Function and Coherence

Beam strain at ω_n was also measured by the root strain gage and displayed separately. The spectral analyzer converts strain gage voltage to a dummy variable of engineering units (EU) and had been programmed such that one EU equals one microstrain ($\mu\epsilon$). A sample plot of strain vs. frequency is shown in Figure 2.4.

Elevated temperature damping measurements were conducted utilizing the "hot box" device developed by Cronauer [Ref. 6]. The device completely encloses the beam, beam clamp, and top of support frame, and measurements can be conducted at temperatures up to approximately 115°C.

Log decrement measurements were conducted by changing signal analyzer configuration to display the output of the root strain gage during the free decay following an impact

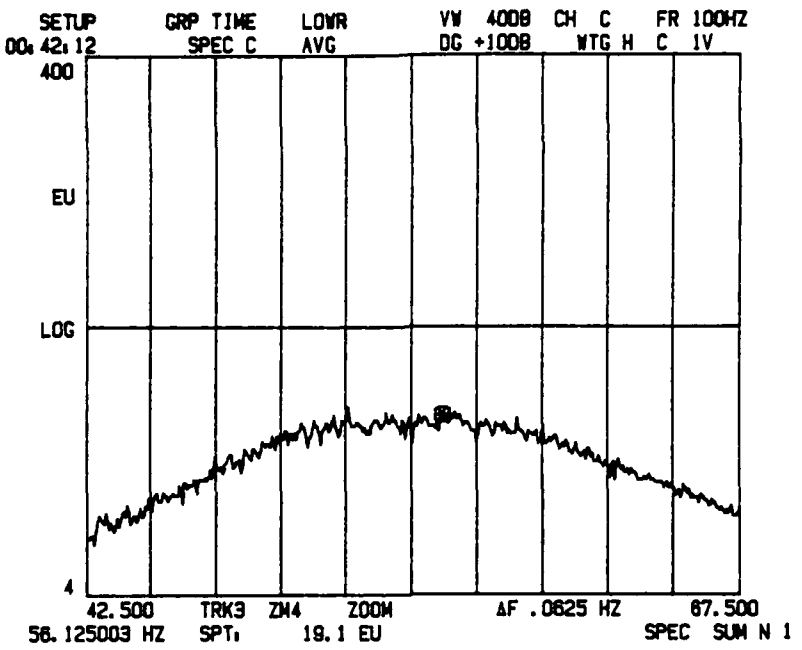

Figure 2.4 Narrow Band Strain Distribution

of the beam. Best results were obtained when impact was with a rod of similar high damping alloy aimed at a point approximately 1/3 the distance from root to free end. Extra reinforcement of the beam clamp was important so that impact energy was not also transmitted through the stinger to the Vibramate exciter, which would otherwise act as a large dashpot and skew response. By varying spectral analyzer set-up and rod impact force, free decay plots of a wide strain range could be obtained, as high as 1000 EU ($\mu\epsilon$) peak amplitude. Specific damping capacity was measured using equation (1.3), and strain data was read directly from the free decay plot. A sample of the plot is shown in Figure 2.5.

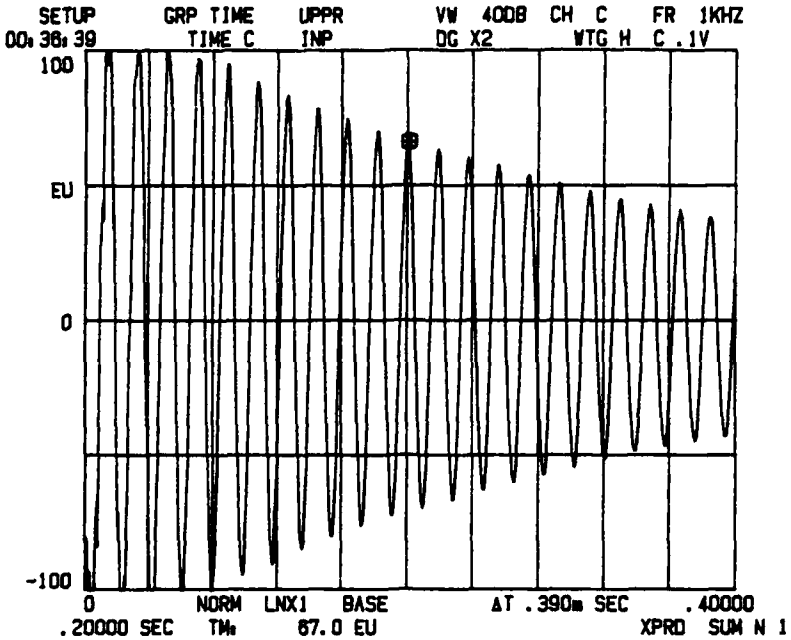

Figure 2.5 Free Decay of Strain

III. RESULTS AND DISCUSSION

A. DAMPING MEASUREMENTS

1. Normalized Band Width

Initial damping capacity measurements were made at room temperature using beams aged at 400°C for 12, 14, 16, 18, and 20 hours. Strain was measured with one strain gage mounted at the beam root (see Figure 2.1) and strain amplitude was varied by adjusting the output of the MB Dynamics 2125 MB power amplifier. Using the amplified signal analyzer random noise signal at maximum output, peak strains were achieved of no more than 13 $\mu\epsilon$. Damping capacity measurements (SDC) with this configuration showed that a 16 hour aging still produced the highest SDC (see Table 2). However, strain levels and corresponding damping capacities were well below the range of interest, and in most cases below the minimum commonly associated with a "high damping" material. Damping measurements were conducted over a period of time (24 hrs) on each aged beam after removal from storage at -22°C but no discernable trend of SDC variation could be observed at these low strain levels.

TABLE 2

PEAK DAMPING CAPACITIES AT LOW STRAINS

Aging Condition (HRS)	Peak SDC (%)	Strain @ Peak ($\mu\epsilon$)
12	13.2	9.9
14	15.4	6.7
16	22.2	9.8
18	13.0	10.9
20	11.6	9.2

Damping capacities also showed little strain dependence, leading to the conclusion that the material was not being

sufficiently stressed to show the expected strain-dependent high damping capacity.

Therefore, modification was made to the beam excitation input via the spectral analyzer set-up which yielded much higher strain levels. Previous trials had utilized a wide range random noise signal which excited the first three beam vibration modes (see Figure 1.1). Strain had been measured and SDC computed at each of the flexure points present in the three modes, yielding a large data base. Since a large data base was not the intent of present research, and since mode one frequencies yielded the largest strain rates, a single root strain gage was utilized, simplifying data collection while maintaining accuracy. In addition, an alternate spectral analyzer set-up generated a pseudo-random signal, consisting of a swept sine wave continuously varied over a desired frequency range. This set-up allowed more concentrated energy to be transmitted to the beam, generating higher strain rates. Beam geometry dictated mode one frequencies in the 50-60 Hz range, therefore a pseudo-random signal from 0-100 Hz was chosen and yielded excellent results. Forced vibration with this method produced strain rates in excess of 60 $\mu\epsilon$.

It was decided to utilize the new method and concentrate further experiments on aging times of 15, 16 and 17 hours. Beams were again solution treated at 800°C and aged at 400°C with procedures outlined in Chapter II. Damping measurements at room temperature were conducted over a 96 hour period following removal from cold storage, with data taken upon removal ("start"), and at +2, +8, +24, and +96 hours. Plots of SDC versus strain for each of the three aging conditions are shown in Figures 3.1, 3.2, and 3.3.

The 16 hour aging condition at 400°C still appears to give highest overall SDC in the strain ranges measured, with peak values of 62.9 % SDC at 66 $\mu\epsilon$ at start, and again 62.9 % SDC at 63.2 $\mu\epsilon$ at +96 hours. The highest SDC for the

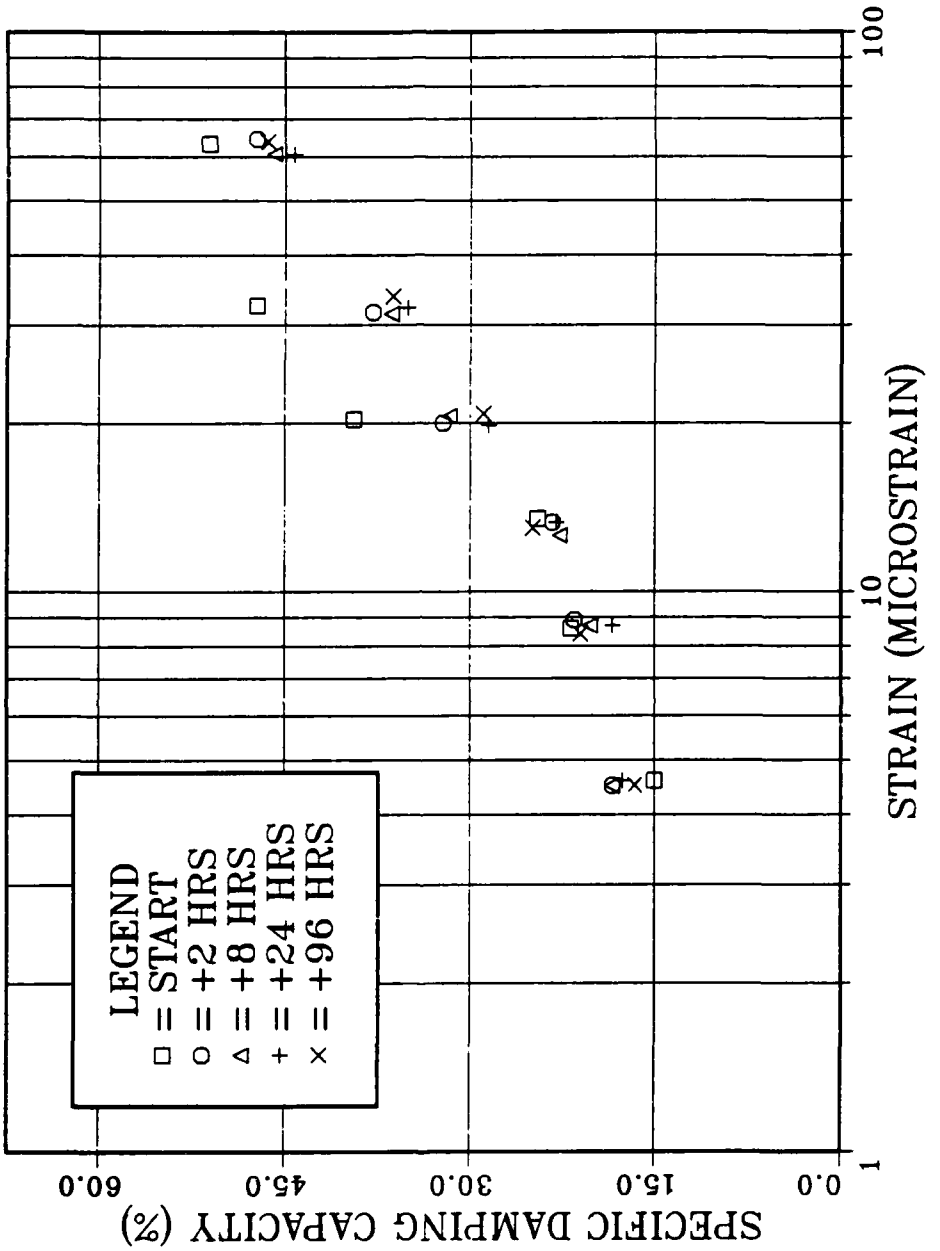

Figure 3.1 Room Temperature SDC vs. Strain for 15 Hour Aging.

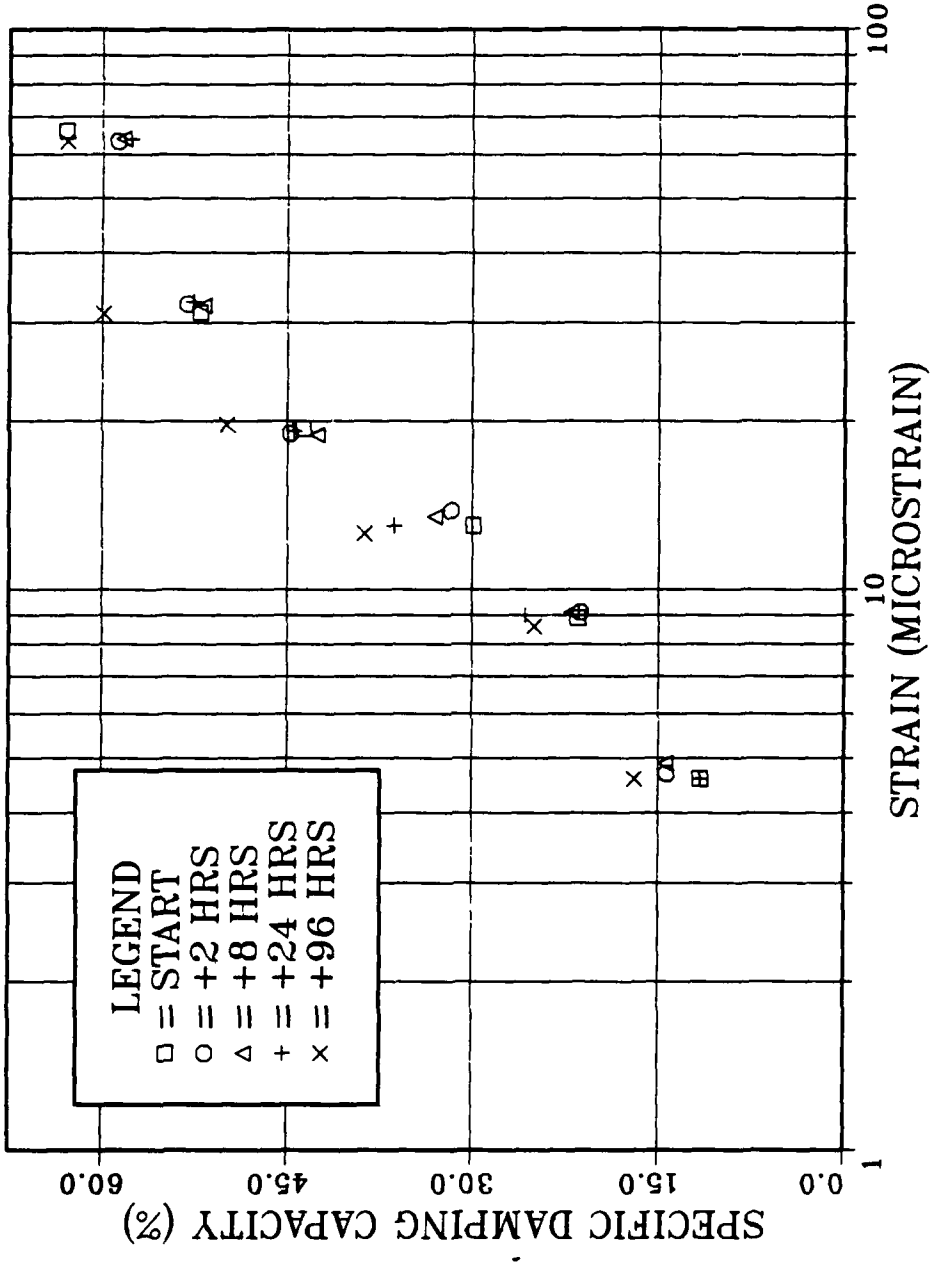

Figure 3.2 Room Temperature SDC vs. Strain for 16 Hour Aging.

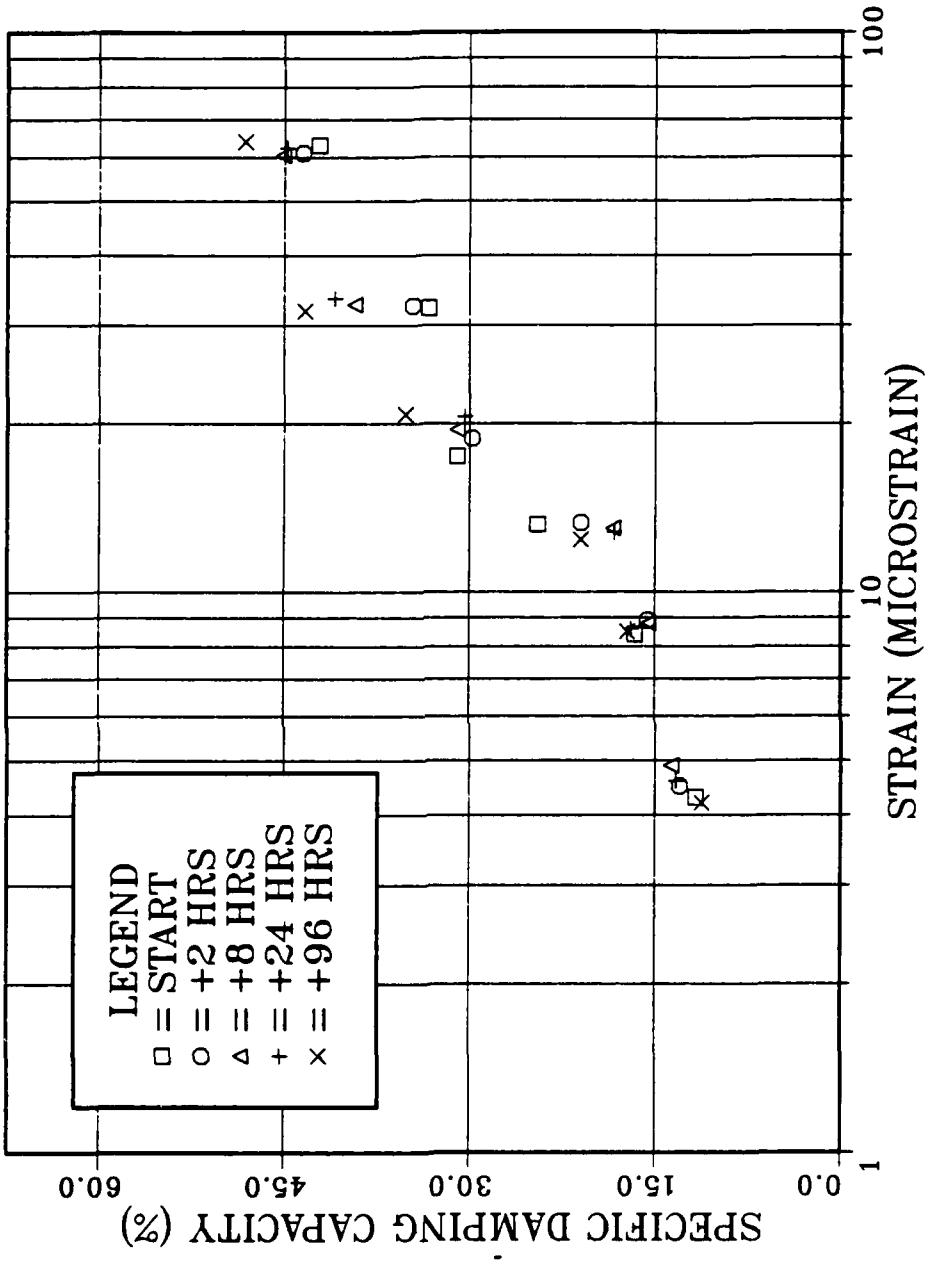

Figure 3.3 Room Temperature SDC vs. Strain for 17 Hour Aging.

15 hour aging condition was 51.1 % at 63.2 $\mu\epsilon$ (start), and for the 17 hour aging condition, 48.2 % SDC at 63 $\mu\epsilon$ (+96 hrs).

SDC trends through +96 hours differed for each of the three aging conditions. For the 15 hour aging condition, there was a general drop in SDC from start to 96 hours, averaging 8.5 % over the strain range. The 16 hour aging condition showed a rather large general increase (20.1 %), but at the largest strains both start and +96 hours the SDC was about the same. The 17 hour aging condition showed a net gain in SDC through 96 hours (7.1 %), although overall damping capacity was less than each of the other two aging conditions.

The average gain in SDC for the 16 hour aged sample after 96 hours at room temperature was somewhat unexpected and may represent a degree of room temperature aging into a better damping condition. The additional room temperature aging that occurs over this period is probably small, so the actual optimum aging time may be slightly longer than 16 hours at 400°C. The 15 and 17 hour aged samples obviously displayed less SDC, the former being apparently underaged and the latter overaged. The 15 hour sample might then be expected to show better damping after 96 hours of room temperature aging, but this did not appear to be the case. It may be that the aging mechanism which leads to high damping is unable to progress at room temperature, possibly not until the alloy reaches a requisite critical stage of transformation. The SDC improvement shown by the 16 hour aged sample after 96 hours at room temperature may then be because the aging mechanism had surpassed this critical stage and could continue progression at room temperature. The 17 hour sample showed slight SDC improvement possibly for the same reason, although the initial overaging causes the overall damping capacity to be relatively low.

Using the elevated temperature test apparatus developed by Cronauer [Reference 6], measurements were conducted on samples initially in each of the three aging conditions (15, 16, and 17 hours at 400°C), and the subsequent effect on SDC of a 100°C test temperature was noted. A calibration check of the apparatus showed that with a nominal controller setting of 120°C, a steady uniform beam temperature of 100°C was achieved in approximately 100 minutes. Therefore, for each beam SDC measurements were taken at room temperature upon removal from cold storage ("start-rm temp"), then allowed to heat for two hours to 100°C before the second set of measurements was taken ("+2-100C"). Elevated temperature was maintained for an additional six hours, when a third SDC measurement was taken ("+8-100C"). The final set of SDC measurements were taken after an immediate cooling to room temperature ("+8-rm temp"). Beam shaking was only conducted while SDC measurements were taken. Figures 3.4, 3.5, and 3.6 show SDC versus strain plots for initial aging conditions of 15, 16, and 17 hours at 400°C respectively.

The effect of the 100°C elevated test temperature and time on the damping capacity of samples from each of the three aging conditions is readily apparent. Within experimental error, no difference in SDC vs. strain can be discerned between the three, whether after two or eight hours at raised temperature. The initial room temperature SDC measurements are comparable to previously measured values, with the 16 hour aging condition again highest. The effect of time at elevated temperature for each can be seen by final room temperature measurements. Both the 16 and 17 hour aged samples show a significant degradation in SDC, while the 15 hour aged sample remains essentially unchanged. It is significant that this unchanged SDC is now higher overall than the degraded SDC of the 16 hour sample. The 17 hour aged sample not only shows an SDC degradation, but a possible peak value of SDC vs. strain is visible in the 30

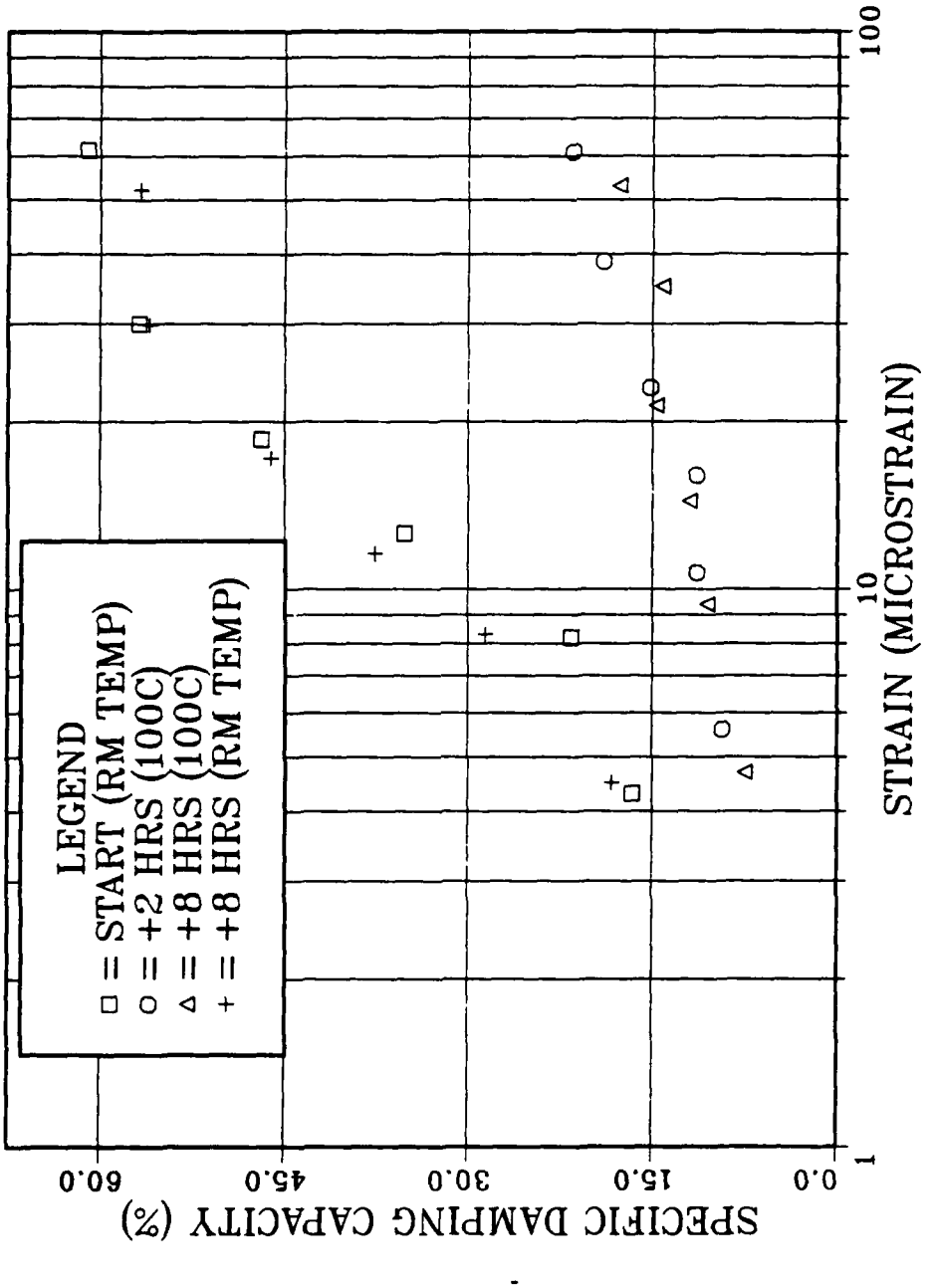

Figure 3.4 Elevated Temperature SDC vs. Strain for 15 Hour Aging.

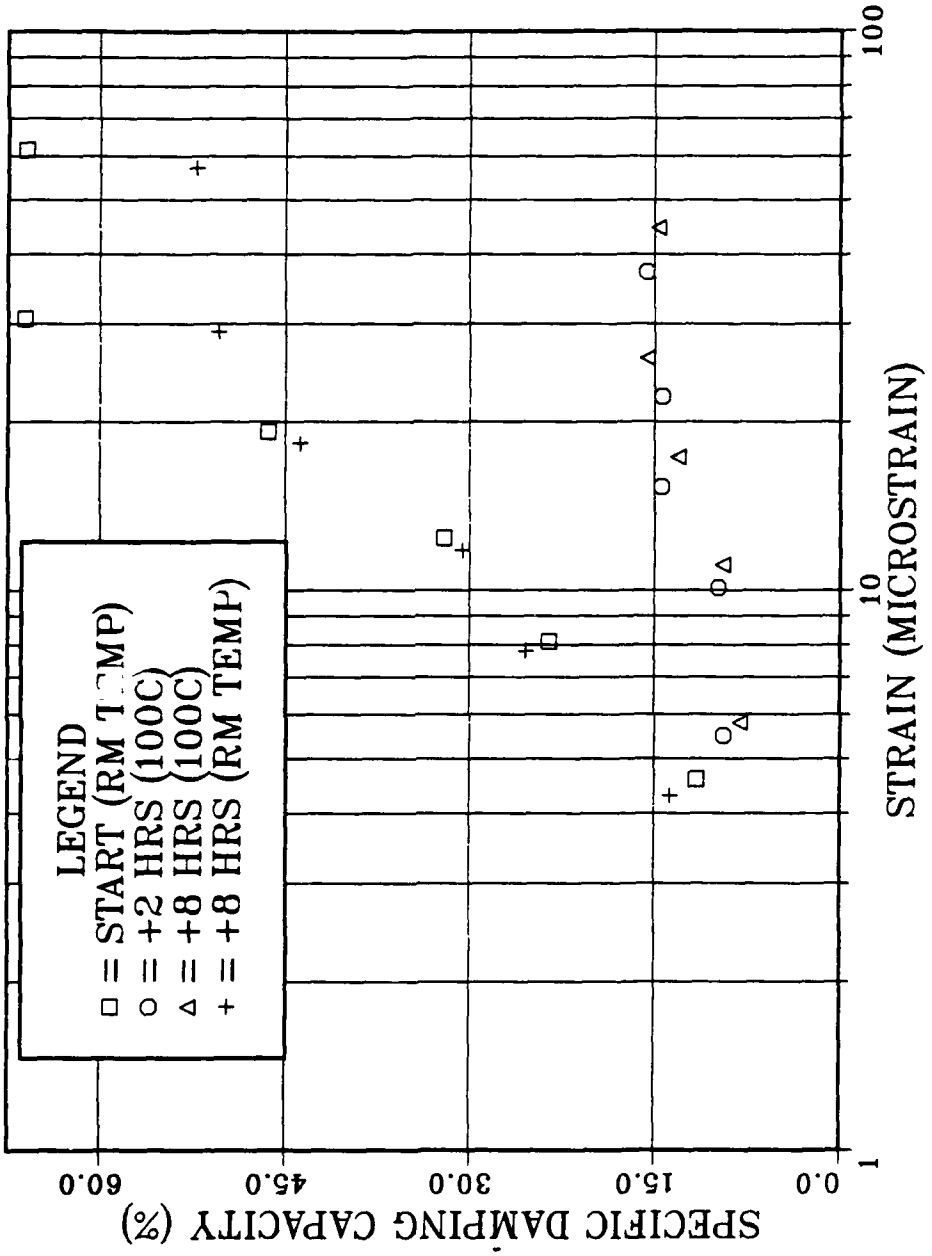

Figure 3.5 Elevated Temperature SDC vs. Strain for 16 Hour Aging

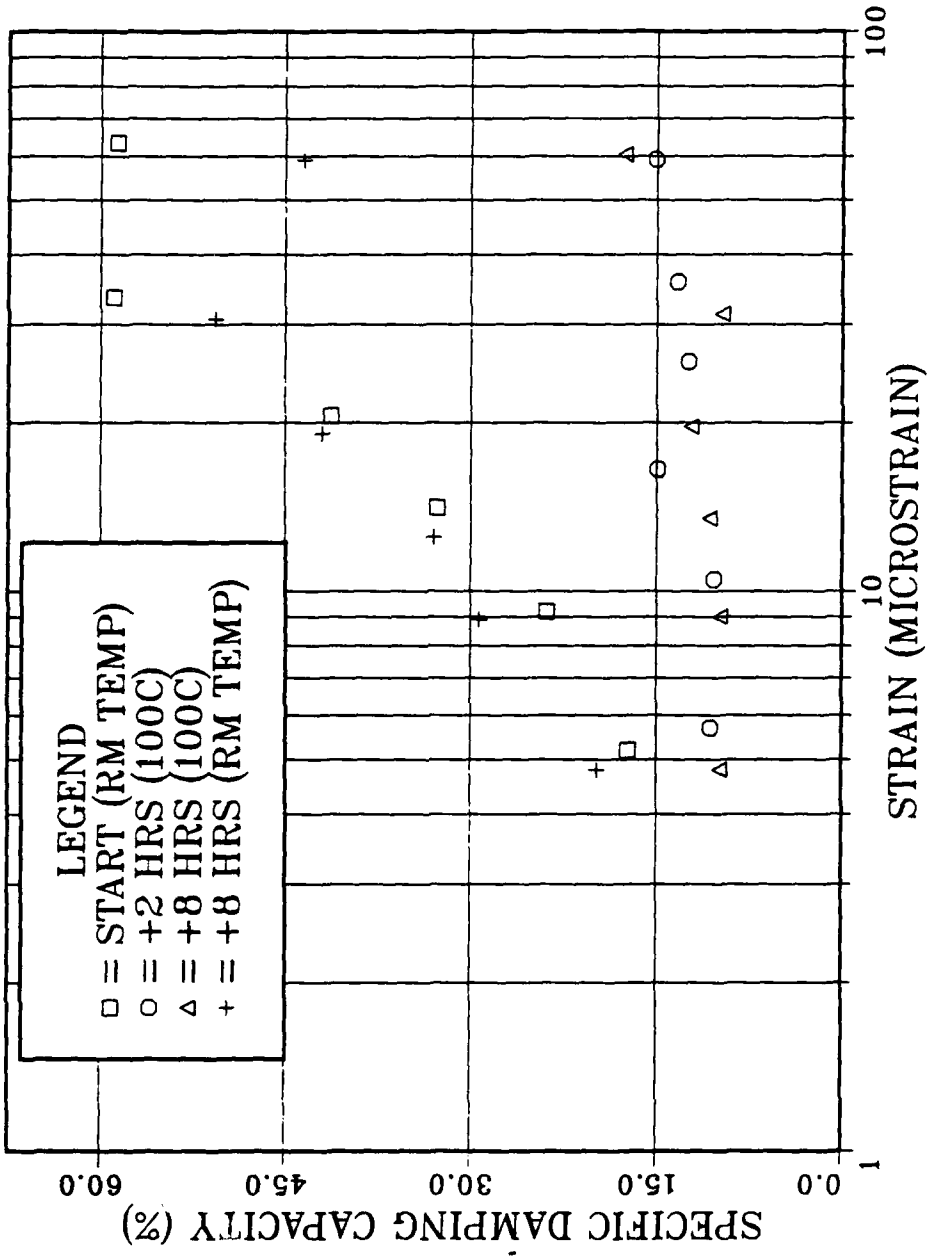

Figure 3.6 Elevated Temperature SDC vs. Strain for 17 Hour Aging

$\mu\epsilon$ range, meaning higher strains may lead to lower SDC. Assuming the damping mechanism had not yet reached the "critical" stage for the 15 hour aged sample in room temperature aging experiments already mentioned, it appears that for the same aging condition at 100°C the mechanism has indeed progressed. For the 16 and 17 hour aged samples, it appears that overaging has taken place.

2. Log Decrement

An investigation was made into the use of an alternate method to quickly and accurately measure the SDC of 53Cu-45Mn-2Al beams. Evaluations of a free decay technique to determine log decrement were conducted using the same beams used for the room temperature SDC measurements. By adjusting the spectral analyzer set-up, it was possible to capture the root strain gage output during the free decay following an impact of the beam, with maximum input strains of up to approximately 1000 $\mu\epsilon$ attainable. Larger impacts and correspondingly higher strains were possible, but were not investigated due to risk of permanent beam deformation.

Each beam was tested immediately after the +24 hour normalized band width measurements were taken, and separate free decay plots were made in ranges of 0-50, 0-100, 0-200, 0-500, and 0-1000 EU ($\mu\epsilon$). An example of one such plot is shown in Figure 2.5. For improved accuracy, values of peak strain amplitude were only recorded above approximately half full scale. SDC values were computed between successive peaks using equation 1.3, each at a strain value defined as the average between the peaks. The plot of SDC versus strain for all three aging conditions is shown in figure 3.7.

Resulting relative SDC vs. strain levels between aging conditions were comparable to those found with the normalized band width method, clearly showing that the 16 hour aging condition produces the highest overall damping.

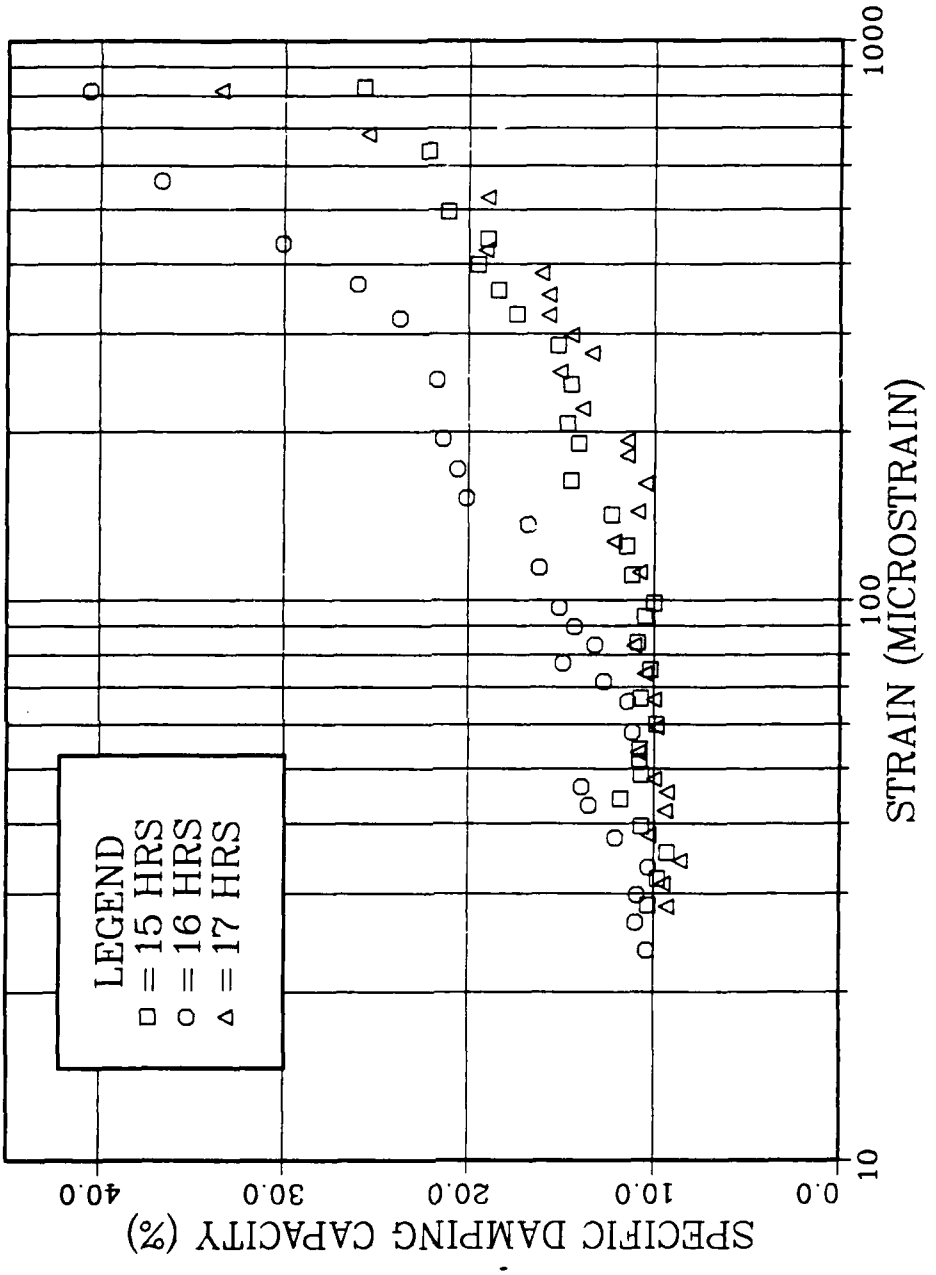

Figure 3.7 SDC vs. Strain, Log Decrement Method

SDC results for the two methods at equivilent strains showed that values were not comparable, and with the log decrement method, maximum SDC values were much lower than the normalized band width method. Two possible reasons for this are hypothesized: (i) the spectral analyzer set up was inaccurate and the displayed strains using this set up were actually much lower, or (ii) the comparison of a normalized band width method, which uses forced vibration, will give inherently higher SDC values than the log decrement method, which uses an impact followed by unforced free decay.

The first of these two hypotheses is not thought to be valid, as the spectral analyzer technical manual [Ref. 39] was thoroughly researched and the company representative was contacted for verification prior to using the technique. Also, this would mean a strain value disparity of almost two orders of magnitude - the peak SDC computed by the log decrement method for the 16 hour aged sample, 40.6 % @ 814.9 $\mu\epsilon$, corresponds to the SDC at a strain of approximately 16 $\mu\epsilon$ computed by normalized band width for the 16 hour aged sample at +24 hours.

Rather, it seems that the second hypothesis is more likely valid and the two methods should not be compared with strict correspondance between SDC values at similar strains. Instead, calculated SDC vs. strain relationships for the respective methods should only be used for comparison with others using the same method.

B. EXAMINATION BY TRANSMISSION ELECTRON MICROSCOPY

1. 53CU-45MN-2AL

Other alloys that display a tweed microstructure are known to show variations in tweed contrast with changes in temperature. One such example was by Schryvers and coworkers [Ref. 34] who showed that the cooling of a Ni-Al alloy brought it into a temperature range of lattice instability and caused a contrast modulation. Perkins [Ref.

40] believes the aging conditions in the present alloy bring about a similar lattice instability at room temperatures, and that the flickering contrast is an observable manifestation of the incipient FCC to FCT transformation in small regions of sufficient Mn content. This observed flickering activity is postulated to be the transformed FCT structures flipping from one orientation to another. It might be hypothesized then that as temperature is increased from room temperature, the unstable Mn-rich clusters should surpass their Néel temperature and return to a stable FCC phase. This should cause two observable effects: (i) flickering should diminish and eventually cease, and (ii) tweed should diminish in clarity, before eventually disappearing, since the localized distortions that had produced the room temperature tweed appearance have disappeared. On the other hand, as temperature is decreased from room temperature, the total amount of Mn-rich regions which have undergone FCC-FCT transition increase to some extent, since structures with lower Mn concentrations, and hence lower Néel temperatures, can now transform. This should manifest itself by either a coarsening of the tweed structure already present, or by formation of new tweedy areas. The effect on flickering would probably be that more total flickering sites become active, although the lowered temperatures may eventually have a detrimental effect on FCT-to-FCT re-orientations.

The exact spatial morphology of the compositional distribution in the aged microstructures has not been determined. It is proposed that the aging conditions for this particular alloy have rendered the structure not into areas of specific Mn-rich and Mn-poor contents, but rather into one where there is a continuous compositional modulation with a wave-like gradient between a Mn-rich content and a Mn-poor content, i.e. spinodal decomposition has occured. This model will be discussed in more detail later.

The development of a tweed microstructure in this alloy has been studied by TEM by two recent researchers, Reskusich [Ref. 4] and Mayes [Ref. 9]. Mayes also discovered the flickering contrast in aged samples which display tweed. Flickering seems to be directly related to tweed development, appearing as longer-range linear flashes in less aged samples (4 to 8 hours), and progressing to smaller localized areas with wide dispersion and greater activity in samples with longer aging (16 hours and up). In order to test these hypotheses, two of the aging conditions which had displayed tweed and had been observed by previous investigators in this laboratory were chosen for observation under in-situ heating and cooling conditions. These two aging conditions were 8 hours and 16 hours aging at 400°C, and were chosen since they tended to display a good range of tweed microstructure and flickering activity. Seven separate samples were observed, five from the 8 hour/400°C aging condition and two from the 16 hour/400°C aging condition. Samples were viewed at temperatures from -163°C to over 80°C. The normal test procedure was to start at room temperature, increase to maximum temperature, cool to minimum temperature, then return to room temperature.

At the initial room temperature, all samples displayed active flickering but varying degrees of tweed. As temperature was raised, all showed a reduction in flickering activity, and complete cessation in the range of 50°C to 70°C. The tweed contrast became "mottled" and disappeared at temperatures slightly above those where the flickering disappeared. As the samples were subsequently re-cooled from maximum temperatures (80°C), tweed and flickering would reappear 10-20°C below the temperatures where they had disappeared. Flickering would continue and even increase intensity below room temperature, through at least -65°C. In one early cooling trial it seemed to then stop, and in other early cooling trials the intensity seemed to diminish

below about -80°C, but these observations may have been due to changes in diffraction conditions. Later observations, made with extreme care to maintain precise two beam conditions, seemed to show virtually no change in flickering upon cooling to the lowest possible temperatures (about-163°C). Characterization of flickering activity is decidedly subjective and until more definitive measurement techniques are available, the description of these variations with temperature must remain relatively general.

Photomicrographs of samples at room temperature and at the high and low temperature extreme are shown in Appendix A. All of these are bright field images, with the sample orientation maintained in a two beam condition with beam direction near [110] and the 022 reflection operating strongly, or beam direction near [100] and the 002 reflection operating strongly. In all cases where an observable tweed was present at room temperature (in itself tenuous at best, depending on exact orientation and tilt), cooling tended to coarsen the structure, while heating would "soften" the tweed, often to extinction. At about -100°C many widely dispersed small basketweave patterns often appeared, each in a small localized section of, and in the same general orientation as the tweed pattern (see Fig. A.8). At-120°C, in one case the structure suddenly changed to a much coarser distinct tweed (compare Figure A.3 to Figure A.4).

As previously mentioned, it is proposed that in these aged alloys there develops a continuous wave-like spatial composition variation between Mn-rich regions and Mn-poor regions throughout the microstructure, due to spinodal decomposition. The minimum and maximum amplitudes of the composition modulation correspond approximately to the Mn contents at either end of the tie line across the miscibility gap at 400°C. Various proposed locations of the miscibility gap have been shown in Figure 1.4. Figure 3.9

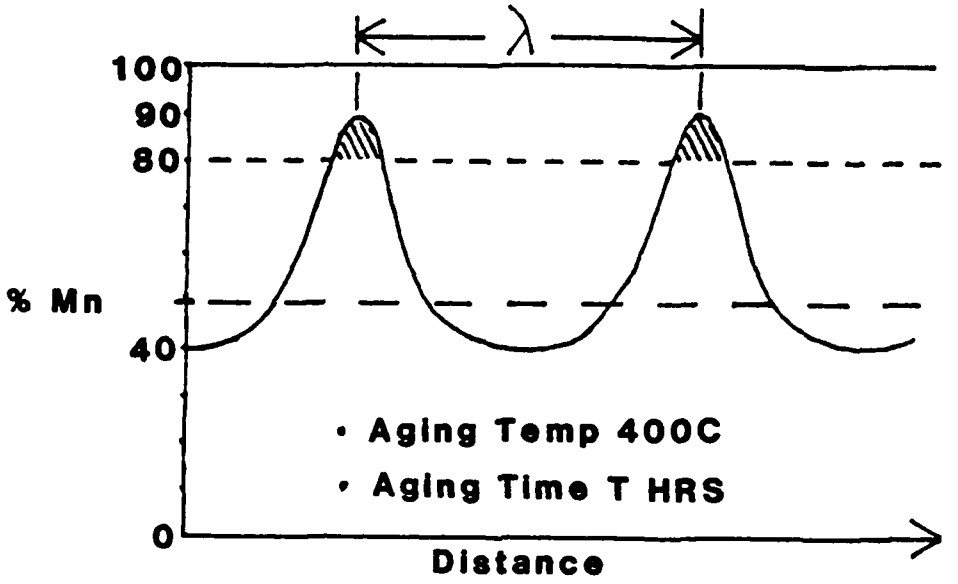

(1) Roughly 40% Mn and 90% Mn at ends of 400°C tie line across miscibility gap.
(2) Shaded areas above 80% Mn represent relative amounts of Mn-rich FCT alloy.
(3) A similar model for the same alloy aged at a longer time would have longer wavelength λ and larger individual shaded areas.

Figure 3.8 Proposed Model of Compositional Variation in Cu-Mn Based Tweed Microstructures

shows a proposed room temperature model for the compositional variation after aging at 400°C for an arbitrary time T. By this model there would exist a periodic distribution of regions in which the Mn content is sufficiently high that FCC-FCT transformation would occur upon cooling to room temperature, and within these regions or near them, flickering may be seen at room temperature. Temperature variations above or below room temperature would be expected to take these regions above or below their local Néel temperature, respectively, with a corresponding effect on tweed contrast and flickering. Increased aging times at a given temperature, say 400°C, would tend to increase the wavelength of the composition modulation, therefore increasing the tweed spacing and perhaps tend to de-couple the Mn-enriched regions.

2. 53.6Cu-46.4Mn Binary

A number of Cu-Mn binary alloy samples of varying compositions were received from Dr. S. Spooner of Oak Ridge National Laboratory. Among these was an alloy of 50Cu-50Mn atomic % composition, or a weight % composition of 53.6Cu-46.4Mn. Since this is nearly identical to the Cu-Mn ratio of the previous alloy, it was decided to observe the binary by TEM under similar preparation and aging conditions (as listed in Chapter II). Table 3 lists the static polish voltages that were used, with the values underlined that produced the best results.

TABLE 3

STATIC POLISH CONDITIONS FOR 53.6CU-46.4MN BINARY ALLOY

Aging Condition @ 400°C (HRS)	Voltage (v)
6	9 11
13	8 10 11
24	10 11
36	8 9 10 11
48	10 11 12

Observations were made in both [110] and [100] beam direction orientations, with 022 and 002 reflections operating strongly in the respective cases. Samples aged 6 hours at 400°C showed no tweed or flickering, and strongly resembled either an as-quenched or 4 hour aged sample of the ternary alloy. With 13 hours of aging at 400°C the structure seemed "mottled" or possibly near-tweed; some flickering was observed, but was extremely rare. Samples aged 24 hours at 400°C were the first to show true tweed, and the flickering activity was quite active. Aging times of 36 and 48 hours at 400°C produced a well developed tweed structure and active flickering, but the banded tweed structure common to similarly aged samples of the previous alloy were not

seen. Photomicrographs of all the aging conditions except 6 hours are shown in Appendix B.

Subjective interpretation of the Cu-Mn binary sample results when compared to the ternary alloy lead to the conclusion that there is a pronounced retardation of the aging process which leads to the development of tweed contrast and flickering. When compared to the results of Mayes, for example, on the ternary alloy, the binary alloy aging times listed in Table 3 (6, 13, 24, 36, and 48 hours at 400°C) are roughly analagous to 53Cu-45Mn-2Al aging times of 4, 8, 12, 16, and 24 hours at 400°C respectively. The binary ages at about half the rate of the ternary alloy. Since the Cu-Mn ratio is nearly equivilent in both alloys, the addition of Al, originally added by the manufacturer to aid in casting and machining properties, is apparently affecting the kinetics of the phase separation transformation and so the development of the tweed contrast microstructure.

An isolated but very interesting observation was made in a weak beam dark field image from the 24 hour/400°C aging condition. Upon close examination of the resulting photomicrograph, a small moiré pattern was discovered. This is an optical phenomenon produced by the superposition of two nearly equivilent repetitive structures, which in this case are assumed to be either overlapping FCT crystals of different orientation, or overlapping FCT and FCC crystals. This provided an opportunity to calculate the tetragonality ratio and compare it to the accepted value. Figure 3.9 shows a portion of the original weak beam image (moiré pattern indicated by arrow) and Figure 3.10 shows an expanded view of the moiré pattern.

Two factors contribute to the orientation of observed microstructural moiré pattern parallel striations: (i) lattice difference with no rotation will give striations normal to the g-vector, and (ii) rotation on the structures

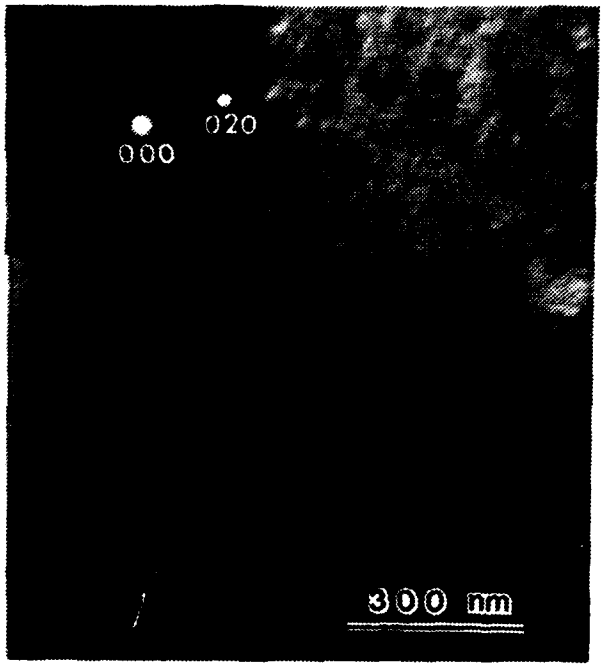

Figure 3.9 Moiré Pattern in 24 Hour Aged 53.6Cu-46.4Mn

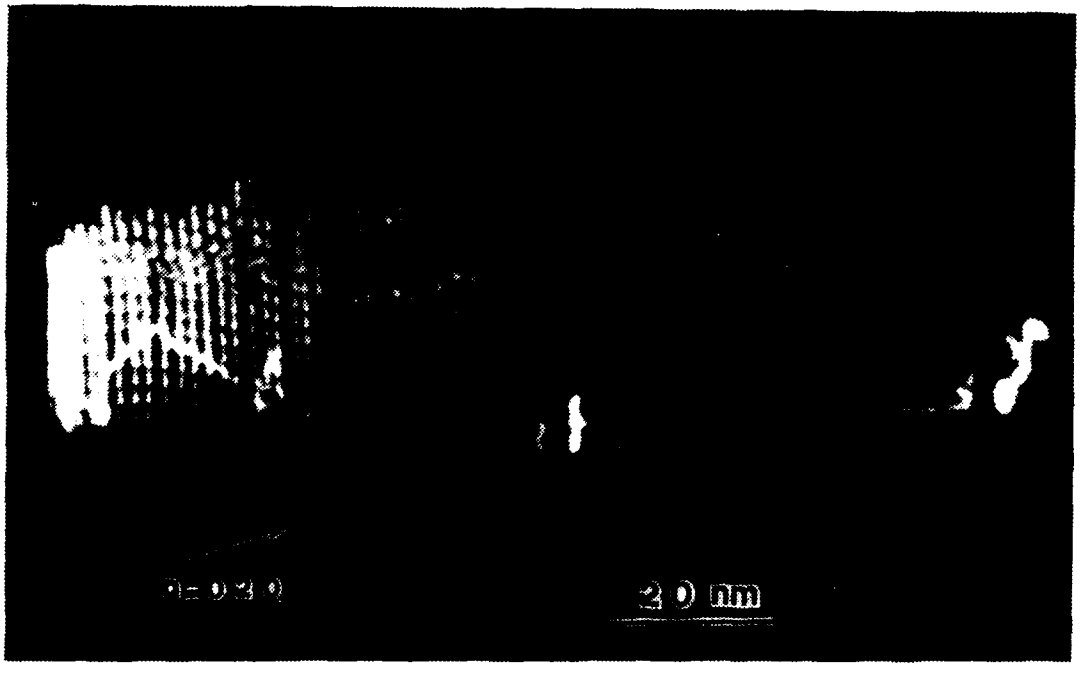

Figure 3.10 Moiré Pattern (close-up)

without lattice difference will give striations parallel to the g-vector [Ref.41 pp. 357-358]. In this case the striations averaged 67° from the g-vector, making the pattern of type (i) above, the difference from 90° due to a slight rotation of the structures magnified by the moiré effect. In the general case where lattice spacings are a_1 and a_2, the spacing D between parallel striations of the moiré pattern is given by [Ref. 41 pg. 359]:

$$D = \frac{(a_1 a_2)}{(a_1 - a_2) * (h^2 + k^2 + l^2)^{\frac{1}{2}}} \qquad (3.1)$$

where h, k, and l are the indices of diffraction of the g-vector.

From Figure 3.10, measured spacings D fell into two consecutive groups, the first with values between 1.6 and 2.4 nm, mean value 1.8 nm, and the second with values between 3.1 and 4.1 nm, mean value 3.4 nm. Solving equation 3.1 for a_2 using a_1 = .375 nm (lattice spacing for 50Cu-50Mn a/o) gives a_2 = .343 nm for case 1 and a_2 = .355 nm above or below an FCC structure of nearly identical orientation for case 2. Dividing these by the lattice spacing a_1 to calculate tetragonality ratios reveals values of 0.92 for case 1 and 0.95 for case 2, each much lower than the expected value of approximately 0.99 [Ref. 27].

The discrepency of calculated tetragonality ratios with the accepted value may be due to flickering. The bright image traversing the field of the moiré pattern in Figure 3.10 is thought to be a captured linear flash type flicker. This may also explain why the moiré spacings are divided into two groups, assuming that the flash may have "jumped" twice during photo exposure.

IV. CONCLUSIONS

Damping capacity measurements conducted on the alloy 53Cu-43Mn-2Al have proven quite fruitful, with useful data concerning optimum aging for peak damping, the effect of elevated temperature on damping capacity, and data on the use of the log decrement technique as an alternate damping measurement method. It was found that the aging time at 400°C which produces the highest room temperature specific damping capacity (SDC) is 16 hours, but a 15 hour aging at the same temperature will give a condition that has higher SDC after 8 hours at 100°C. SDC was shown to drop by an average of almost 70% when the alloy was used at 100°C instead of room temperature. The log decrement technique was shown to be accurate, but only when compared with other specimens tested by the same method. When compared to the normalized band width method at comparable strains, values of SDC for the log decrement method were lower by almost two thirds. Absolute peak SDC values for the log decrement method (at strains over an order of magnitude higher) were still about two thirds of those calculated by the normalized band width method.

Transmission electron microscopy (TEM) yielded much information on the effects of temperature variation on aged 53Cu-45Mn-2Al, both on the tweed microstructure and "flickering" effect. It was shown that raising the temperature from ambient conditions to a maximum of over 80°C causes the tweed microstructure to vanish and flickering to disappear, probably since Mn-rich FCT regions have transformed back to FCC. Cooling from room temperature to a minimum of -163°C caused tweed structures to coarsen and improve in clarity, and had little effect on flickering.

TEM studies of the binary alloy 53.6Cu-46.4Mn showed that at aging conditions similar to the ternary alloy,

development of tweed microstructure and flickering lagged behind that of the ternary alloy, by as much as 50%, possibly indicating a strong kinetic effect of the Al in the ternary alloy.

V. RECOMMENDATIONS FOR FURTHER STUDY

The following recommendations for further research are provided, presented under the general headings of damping studies and transmission electron microscopy (TEM) studies.

Damping studies:

a. An alternate damping measurement technique for use on small specimens should be investigated. A wide variety of variously aged alloys are expected to be investigated and supply may be limited.

b. More investigation into damping capacities at accurately maintained elevated temperatures may provide useful data for correlation to microstrucural development observations at corresponding temperatures.

TEM:

a. More in-depth characterization of flickering activity is warranted. For example, a high resolution video system could be used and successive frames of the video presented for photographic documentation. A system to measure and record flickering frequencies would be useful, especially in conjunction with elevated and lowered temperature studies.

b. Microstructural development studies done at temperatures other than 400°C would provide information concerning the proposed spatial composition model.

c. Studies of Cu-Mn binary alloys with varied compositions may provide further insight on tweed development and the effects of Al in 53Cu-45Mn-2Al.

APPENDIX A

TRANSMISSION ELECTRON MICROGRAPHS OF AGED 53CU-45MN-2AL AT VARIOUS TEMPERATURES

The following are transmission electron micrographs of 53Cu45Mn2Al alloy aged at 400°C for 8 or 16 hours at various temperatures (orientation indicated).

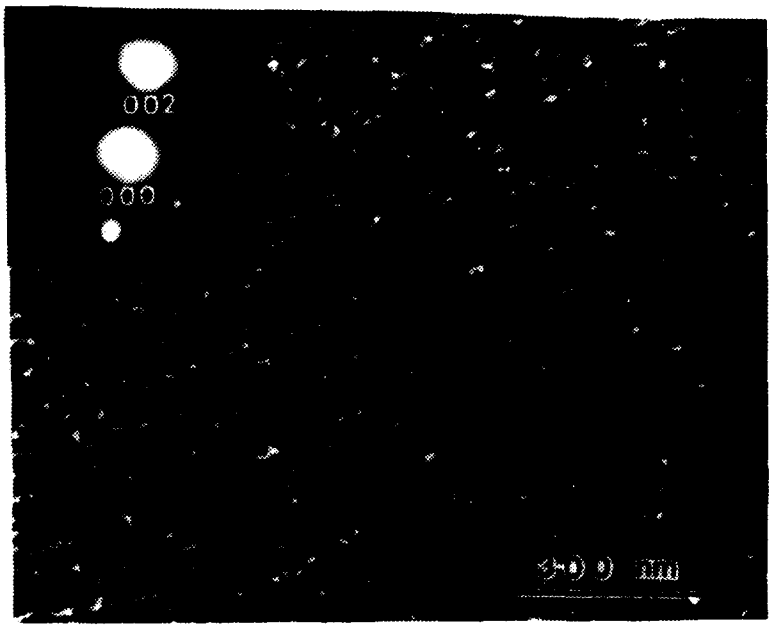

Figure A.1 8 Hours Aging, 21°C, (110)

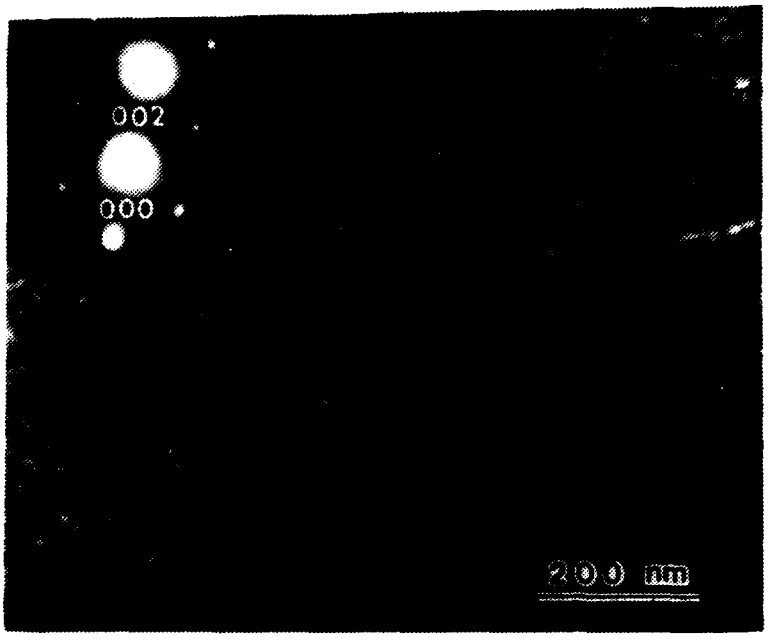

Figure A.2 8 Hours Aging, 81°C, (110)

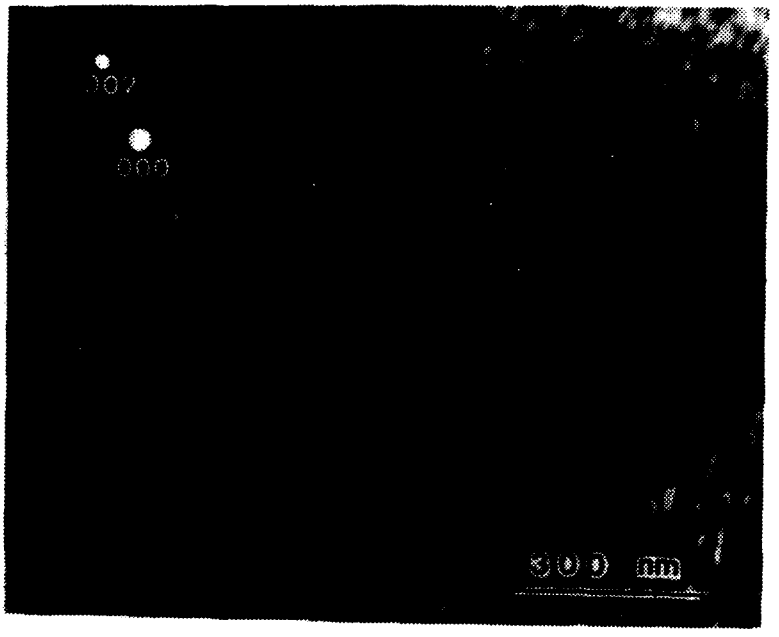

Figure A.3 8 Hours Aging, -157°C, (100)

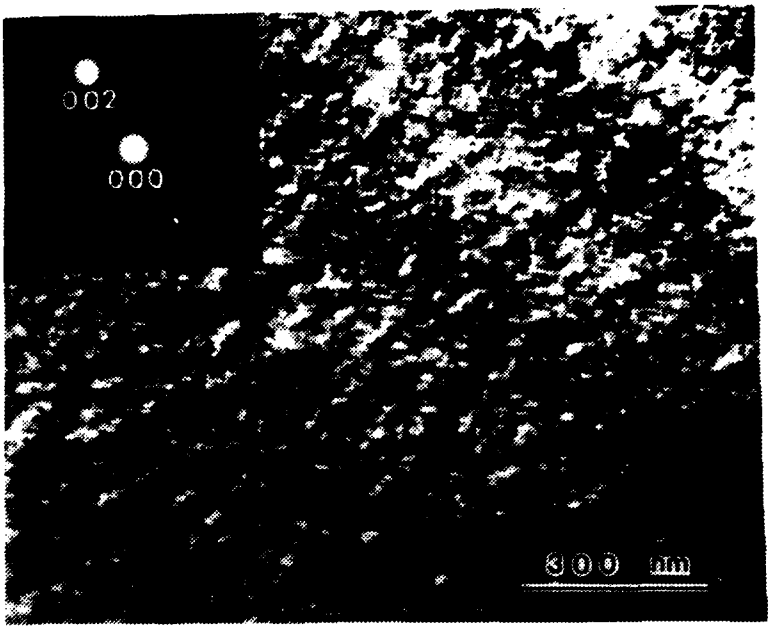

Figure A.4 8 Hours Aging, 21°C, (100)

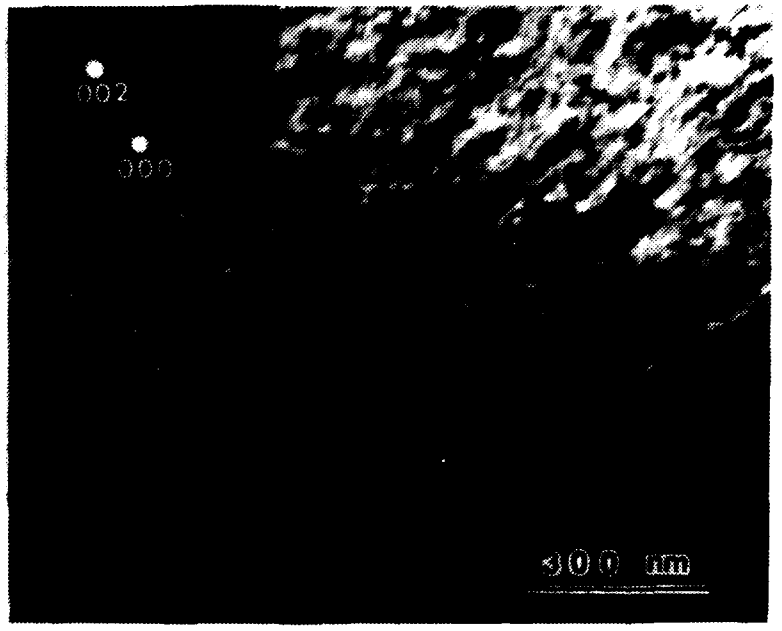

Figure A.5 8 Hours Aging, 82°C, (100)

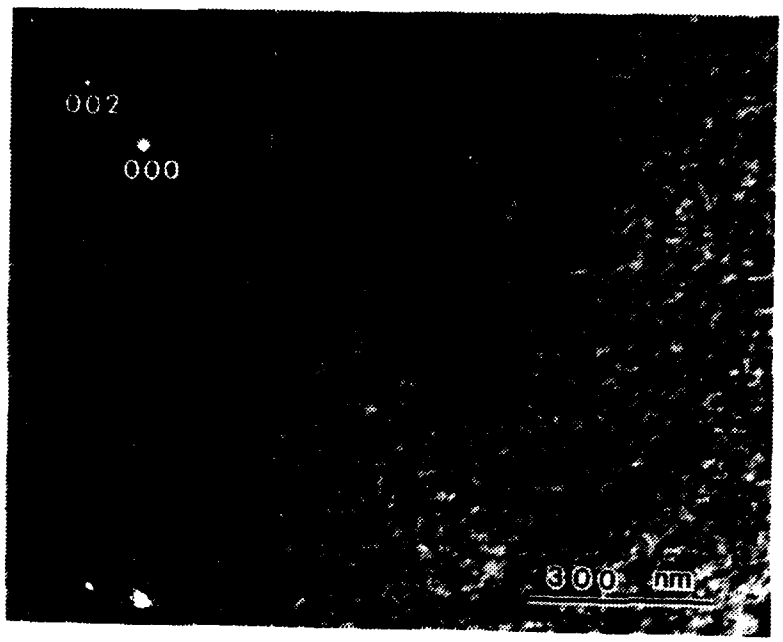

Figure A.6 16 Hours Aging, -140°C, (110)

Figure A.7 16 Hours Aging, 82°C, (110)

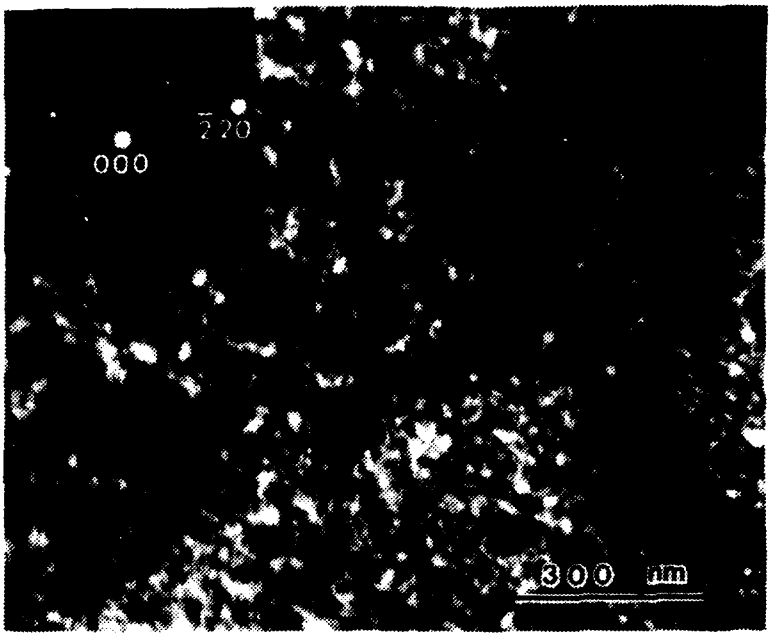

Figure A.8 16 Hours Aging, -163°C, (110)

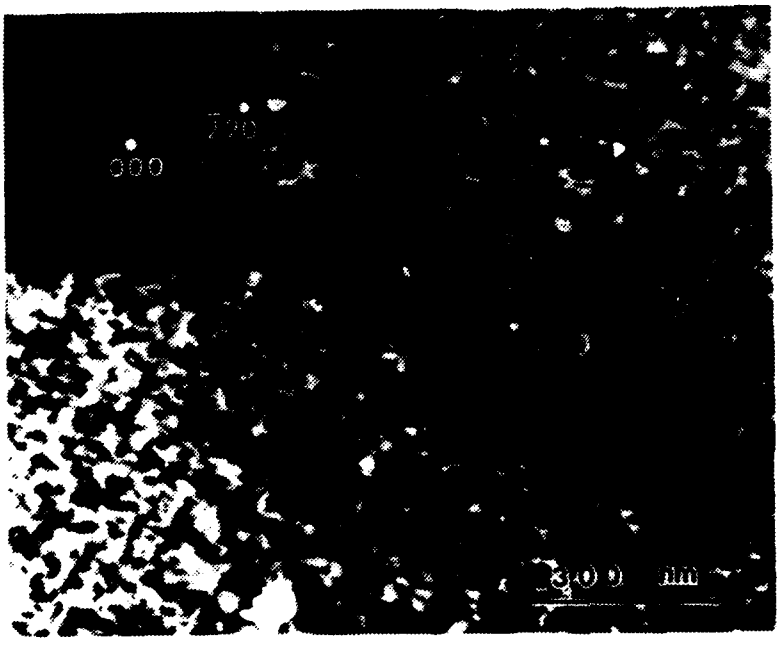

Figure A.9 16 Hours Aging, 21°C, (110)

APPENDIX B

TRANSMISSION ELECTRON MICROGRAPHS OF 54.6CU-46.4MN BINARY ALLOY AGED AT VARIOUS TIMES

The following are transmission electron micrographs of 54.6Cu46.4Mn binary alloy aged at 400°C for 13, 24, 36, or 48 hours (orientation indicated).

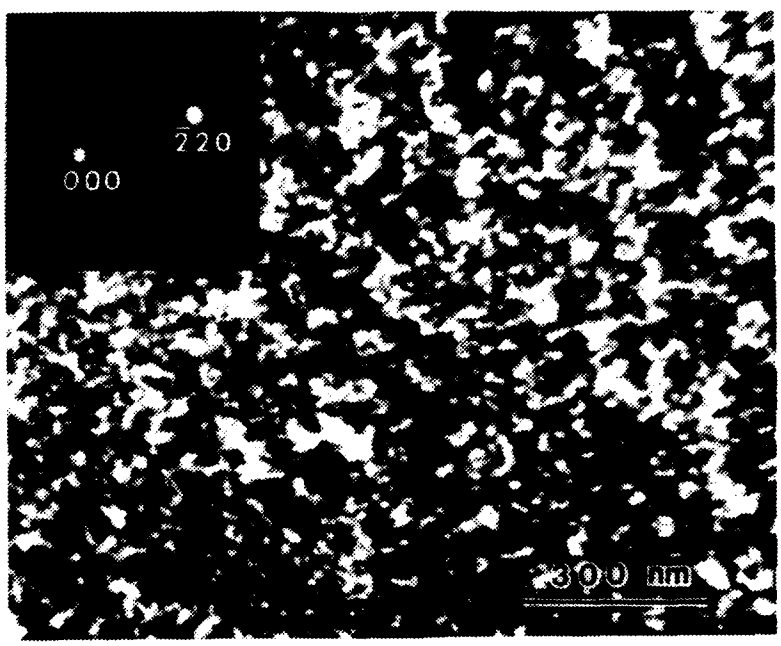

Figure B.1 13 Hours Aging, (110)

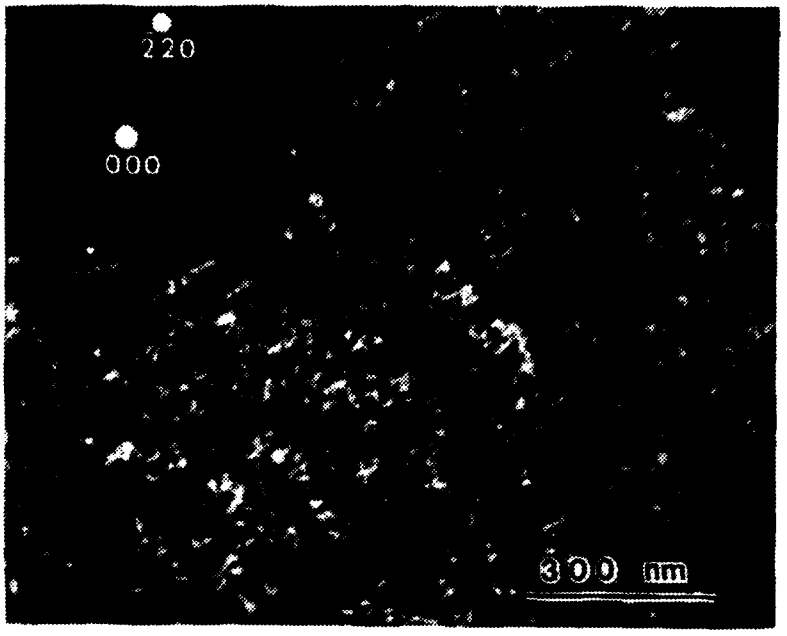

Figure B.2 24 Hours Aging, (110)

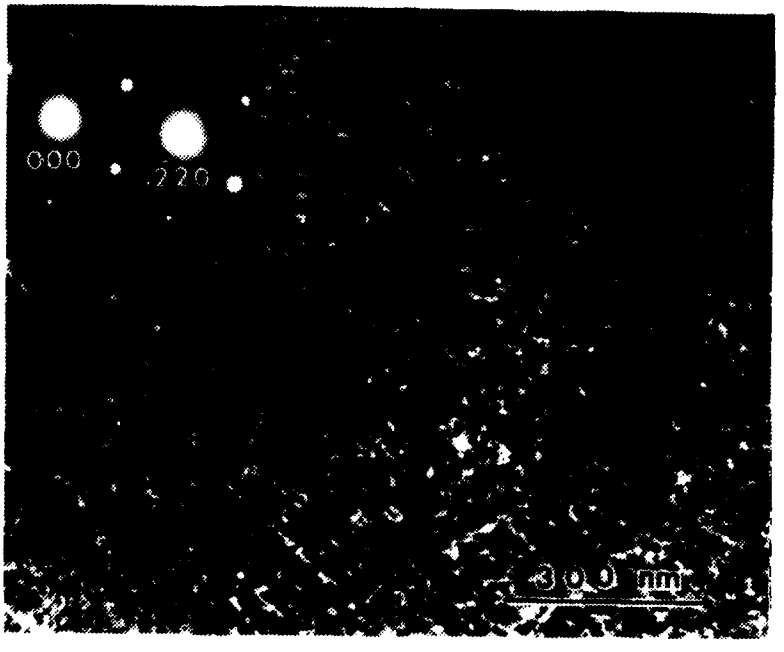

Figure B.3 36 Hours Aging, (110)

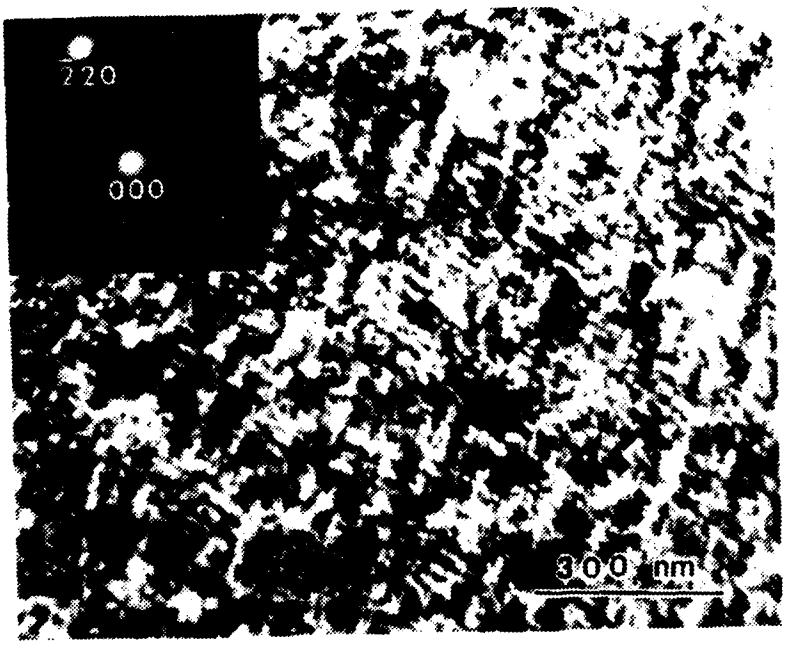

Figure B.4 48 Hours Aging, (110)

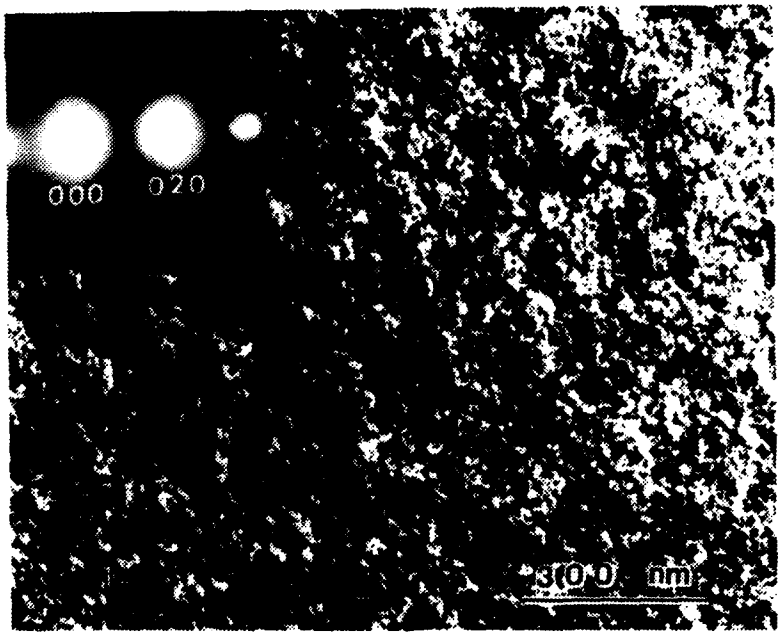

Figure B.5 13 Hours Aging, (100)

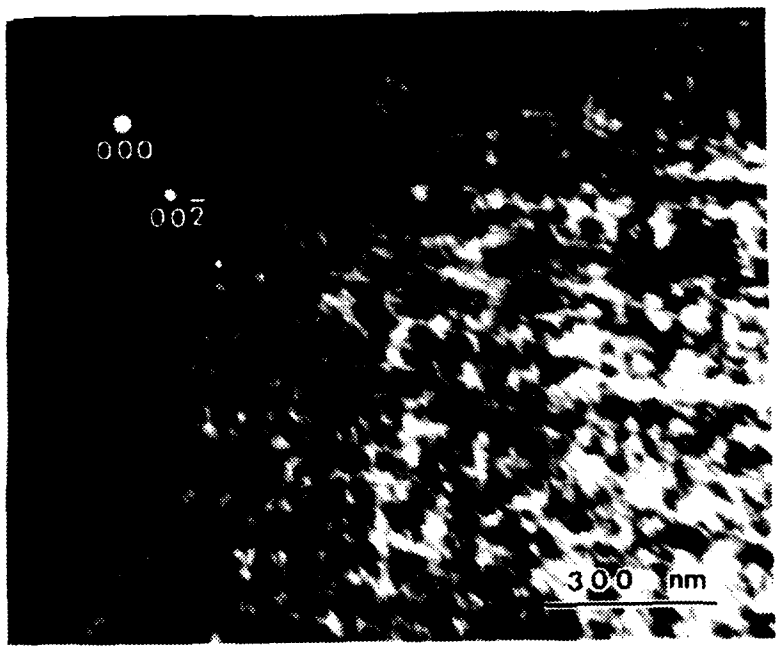

Figure B.6 24 Hours Aging, (100)

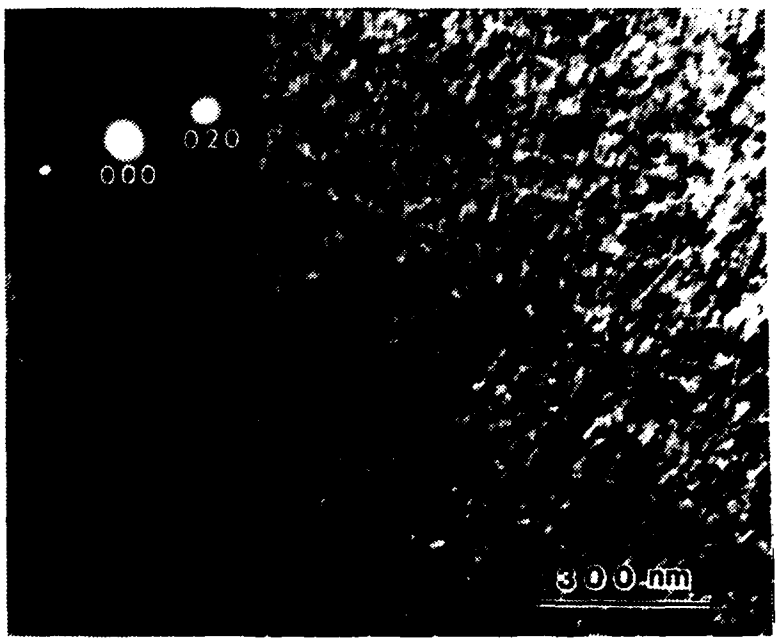

Figure B.7 36 Hours Aging, (100)

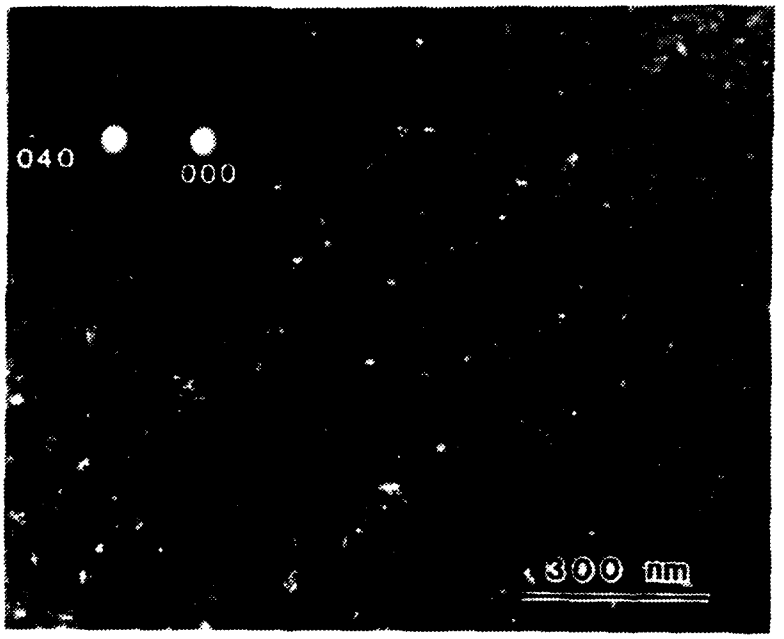

Figure B.8 48 Hours Aging, (100)

LIST OF REFERENCES

1. Schetky, L. M. and Perkins, J., "The 'Quiet' Alloys", Machine Design, pp. 202-206, 6 April 1978.

2. Thomson, W. T., Theory of Vibrations with Applications, Prentice-Hall, Inc., 1981.

3. Reed-Hill, R.E., Physical Metallurgical Principles, Brooks/Cole Engineering Div., 1973.

4. Reskusich, J. and Perkins, J., Damping Behavior of Incramute: Strain Dependence and Heat Treatment Effects, Naval Postgraduate School Technical Report No. NPS 69-87-001, Monterey, CA, September 1986.

5. Dew, D.D., Strain Dependent Damping Characteristics of a High Damping Mn-Cu Alloy, M.S. and M.E. Thesis, Naval Postgraduate School, Monterey, CA, September 1986.

6. Cronauer, J. and Perkins, J., Damping Behavior of a Ti-Ni Shape Memory Alloy: Comparison with Cu-Mn Based and Fe-Cr Based High Damping Alloys, Naval Postgraduate School Technical Report No. NPS 69-87-006, Monterey, CA, June 1987.

7. Ritchie, I., Pan, Z.-L., Sprungmann, K.W., Schmidt, H.K., and Dutton, R., "High Damping Alloys - The Metal lurgists Cure for Unwanted Vibrations", Canadian Metallugical Quarterly 1987, 1987, in press.

8. Dean, R.S., Potter, E.V., and Long, J.R., "Properties of Transitional Structures in Cu-Mn Alloys", Transactions ASM, Vol. 34, pp. 465-500, 1945.

9. Mayes, L.L., An Electron Microscopy Study of Tweed Microstructures and Premartensitic Effects in High Damping 53Cu45Mn2Al Alloy, M.S. Thesis, Naval Postgraduate School, Monterey, CA, March 1988.

10. Smith, J. H. and Vance, E. R., "Decomposition of Gamma-Phase Manganese Copper Alloys", Journal of Applied Physics, Vol. 40, No. 12, pp. 4853-4858, 1969.

11. Sugimoto, K., Mori, T. and Shiode, S., "Effect of Composition on the Internal Friction and Young's Modulus in Gamma-Phase Mn-Cu Alloys", Metal Science Journal, Vol. 7, pp. 103-108, 1973.

12. Meneghetti, D. and Sidhu, S. S., "Magnetic Structures in Copper-Manganese Alloys", Physical Review, Vol. 105, No. 1, pp. 130-135, 1957.

13. Street, R., "Magnetic Properties of Manganese Copper Alloys", Journal of Applied Physics, Supplement to Vol. 31, No. 5, pp. 310S-317S, 1960.

14. Schwaneke, A. E. and Jensen, J. W., "Magnetic Susceptibility and Internal Friction of Tetragonal Manganese-Copper Alloys Containing 70 Percent Manganese", Journal of Applied Physics, Supplement to Vol. 33, No. 3, pp. 1350-1351, 1962.

15. Bacon, G. E., Dunmur, I. W., Smith, J. H. and Street, R., "The Antiferromagnetism of Manganese Copper Alloys", Proceeding of the Royal Society of London, Series A, Vol. 241, pp. 223-238, 1957.

16. Vitek, J. M. and Warlimont, H., "On a Metastable Miscibility Gap in Gamma-Mn-Cu Alloys and the Origin of their High Damping Capacity", Metal Science, Vol. 10, No. 1, pp. 7-13, 1976.

17. Vintaykin, Ye. Z., Dmitriyev, V. B. and Udovenko, V. A., "Spinodal Decomposition in Manganese-Copper Alloys", Phys. Met. Metall., Vol. 46, No. 4, pp. 97-107, 1978.

18. Basinski, Z. S. and Christian, J. W., "The Cubic-Tetragonal Transformation in Manganese-Copper Alloys", Journal of the Institute of Metals, Vol. 80, pp. 659-666, 1951-52.

19. Bichinashvili, A. I., Vintaykin, Ye. Z., Litvin, D. F. and Udovenko, V. A., "X-ray Investigation of the FCC to FCT Transformation in Manganese-Copper Alloys", Physical Metallurgy and Metallography (in Russian, Fiz. Metal. Metalloved.), Vol. 41, No. 1, pp. 112-117, 1976.

20. Worrell, F. T., "Twinning in Tetragonal Alloys of Copper and Manganese", Journal of Applied Physics, Vol. 19, pp. 929-933, 1948.

21. Makhurane, P. and Gaunt, P., "Lattice Distortions, Elasticity and Antiferromagnetic Order in Copper-Manganese Alloys" J. Phys. C (Solid St. Phys.), Ser. 2, Vol. 2, 1969.

22. Nittono, O., Satoh, T. and Koyama, Y., "Cubic-Tetragonal Transformation and Reversible Shape Memory Effect in Manganese-Copper Alloys", Transactions of the Japan Institute of Metals, Vol. 22, No. 4, pp. 225-236, 1981.

23. Vintaykin, Ye. Z., Litvin, D. F., and Udovenko, V. A., "Fine Crystalline Structure in Highly Shock-Absorbing Alloys of Manganese and Copper", Physical Metallurgy and Metallography (in Russian, Fiz. Metal. Metalloved.), Vol. 37, No. 6, pp. 1228-1237, 1974.

24. Spooner, S., Gaulin, B. D. and Morii, Y., "An In-situ Study of Decomposition in Manganese Rich Copper Manganese Alloys with Neutron Scattering", Manuscript, Cambridge, 1987.

25. Hedley, J. A., "The Mechanism of Damping in Manganese-Copper Alloys", Metal Science Journal, Vol. 2, pp. 129-137, 1968.

26. Men'shikov, A. Z., Favstov, Yu. K., Kochetkova, L. P., Konoplev, L. M. and Dorofeyev, Yu. A., "Structural Transformations During the Tempering of High-Damping Manganese-Copper Alloys", Physical Metallurgy and Metallography (in Russian, Fiz. Metal. Metalloved.), Vol. 39, No. 4, pp. 793-800, 1975.

27. Butler, E. P. and Kelly, P. M., "High Damping Capacity Manganese-Copper Alloys. Part 1 - Metallography", Transactions of the Metallurgical Society of AIME, Vol. 242, pp. 2099-2106, 1968.

28. Siefert, A. V. and Worrell, F. T., "The Role of Tetragonal Twins in the Internal Friction of Copper Manganese Alloys", Journal of Applied Physics, Vol. 22, No. 10, pp. 1257-1259, 1951.

29. Birchon, D., Bromley, D. E. and Healey, D., "Mechanism of Energy Dissipation in High-Damping-Capacity Manganese-Copper Alloys", Metal Science Journal, Vol. 2, pp. 41-46, 1968.

30. Tanner, L.E.., "Diffraction Contrast from Elastic Shear Strains due to Coherent Phases", Philosophical Magazine, Vol. 14, No. 127, p. 111, 1966.

31. Robertson, I. M. and Wayman, C. M., "Tweed Microstructures: I. Characterization of Beta-NiAl", Philosophical Magazine A, Vol. 48, No. 3, pp. 421- 442, 1983.

32. Delaey, L., Perkins, A. J. and Massalski, T. B., "Review: On the Structure and Microstructure of Quenched Beta-Brass Type Alloys", Journal of Materials Science, Vol. 7, pp. 1197-1215, 1972.

33. Tanner, L. E., "The Ordering Transformation in Ni_2V", Acta Metallurgica, Vol. 20, pp. 1197-1227, 1972.

34. Schryvers, D., Tanner, L. E. and Tendeloo, G. V., "Premartensitic Microstructures as Seen in the High Resolution Electron Microscope: A Study of a Ni-Al Alloy", NATO/ASI Symposium on Phase Stability, Crete, June 1984, A. Gonis and M. Stocks Editors (Martinus Nijhoff Publishing, Dordrecht, Netherlands), 1988, in press.

35. Zener, C.,"Contributions to the Theory of Beta-Phase Alloys" Physical Review, Vol. 71, p. 846, 1947.

36. Tanner, L. E., Private Communication, 1988.

37. Yeomens, S. R. and McCormick, P. G., "An Investigation of Precipitation and Strengthening in Age-hardening Copper-Manganese Alloys", Materials Science and Engineering, Vol. 34, pp. 101-109, 1978.

38. Shimizu, K., Okumura, Y. and Kubo, H., "Crystallographic and Morphological Studies on the FCT to FCT Transformation in Mn-Cu Alloys", Transactions of the Japan Institute of Metals, Vol. 23, No. 2, pp. 53-59, 1982.

39. Scientific Atlanta Spectral Dynamics Division, "Operator's Manual, SD380Z Signal Analyzer," 1986.

40. Perkins, J., Mayes, L.L., and Yamashita, T., "Flickering Contrast in TEM Images of Tweed Microstructures in an Aged 53Cu-45Mn-2Al Alloy", Scripta Metallugica, 1988, in press.

41. Hirsch, P. B., Howie, A., Nicholson, R.B., Pashley, D.W., Whelan, M.J., Electron Microscopy of Thin Crystals, The Butterworth Group, 1971.

INITIAL DISTRIBUTION LIST

		No. Copies
1.	Defense Technical Information Center Cameron Station Alexandria, Virginia 22304-6145	2
2.	Library, Code 0142 Naval Postgraduate School Monterey, California 93943-5002	2
3.	Research Administration, Code 012 Naval Postgraduate School Monterey, California 93943-5000	1
4.	Department Chairman, Code 69Hy Department of Mechanical Engineering Naval Postgraduate School Monterey, California 93943-5000	1
5.	Professor A. J. Perkins, Code 69Ps Department of Mechanical Engineering Naval Postgraduate School Monterey, California 93943-5000	8
6.	Mr. Robert Hardy, Code 2803 David W. Taylor Research Center Annapolis, Maryland 21402	3
7.	Ms. Cathy Wong, Code 2812 David W. Taylor Research Center Annapolis, Maryland 21402	5
8.	LT Joseph P. Heil, USN 1553 Eton Way Crofton, Maryland 21114	5
9.	Mr. A. G. S. Morton, Code 2813 David W. Taylor Research Center Annapolis, Maryland 21402	1
10.	Dean of Science and Engineering, Code 06 Naval Postgraduate School Monterey, California 93943-5000	1
11.	Mr. Charles Zanis, Code 2844 Naval Sea Systems Command Washington D.C. 20352	1
12.	Mr. V. J. Castelli, Code 2844 David W. Taylor Research Center Annapolis, Maryland 21402	1
13.	Lcdr Wallace M. Elger, Code 05MB Naval Sea Systems Command Washington D.C. 20362-5101	1